Spectroscopic evidence for direct flavin-flavin contact in a bifurcating electron transfer flavoprotein

H. Diessel Duan[1], Nishya Mohamed-Raseek[1] and Anne-Frances Miller[1*]

[1]Department of Chemistry, University of Kentucky, Lexington, KY 40506

Running title: 726 nm CT band suggests direct flavin-flavin contact

*To whom correspondence should be addressed: Anne-Frances Miller, Department of Chemistry, University of Kentucky, Lexington KY 40506-0055 U.S.A. Tel (859) 257-9349, Email afmill3r2@gmail.com

Key Words: Flavin, Flavoprotein, ETF, FixAB, Charge transfer, Electron transfer, Electron bifurcation, Flavin dimer, Computation

Abstract

A remarkable charge transfer (CT) band is described in the bifurcating electron transfer flavoprotein (Bf-ETF) from *Rhodopseudomonas palustris* (*Rpa*ETF). *Rpa*ETF contains two FADs that play contrasting roles in electron bifurcation. The Bf-FAD accepts electrons pairwise from NADH, directs one to a lower-*E*° carrier and the other to the higher-*E*° electron transfer FAD (ET-FAD). Previous work noted that the CT band at 726 nm formed when ET-FAD was reduced and Bf-FAD was oxidized, suggesting that both flavins participate. However, existing crystal structures place them too far apart to interact directly. We present biochemical experiments addressing this conundrum and elucidating the nature of this CT species. We observed that *Rpa*ETF missing either FAD lacked the 726 nm band. Site-directed mutagenesis near either FAD produced altered yields of the CT species, supporting involvement of both flavins. The residue substitutions did not alter the absorption maximum of the signal, ruling out contributions from residue orbitals. Instead, we propose that the residue identities modulate the population of a protein conformation that brings the ET-flavin and Bf-flavin into direct contact, explaining the 726 nm band based on a CT complex of reduced ET-FAD and oxidized Bf-FAD. This is corroborated by persistence of the 726 nm species during gentle protein denaturation and simple density functional theory calculations of flavin dimers. Although such a CT complex has been demonstrated for free flavins, this may be the first observation of such, to our knowledge, in an enzyme. Thus, Bf-ETFs may optimize electron transfer efficiency by enabling direct flavin-flavin contact.

Introduction

Electron transfer is central to energy metabolism in all kingdoms of life. Of the redox cofactors used, FMN and FAD are among the most versatile (1,2). The flavin moiety is inherently poised between one-electron and two-electron reactivities by the tunable stability of the flavin's semiquinone states (3) and the flavin can couple electron transfer to proton transfer (4). At one extreme, dehydrogenases transfer pairs of electrons as hydride between NAD(P)H and closed-shell metabolites (5,6). The striking example of 2-naphthoyl-CoA reductase transfers a strongly reducing hydride (7). In contrast, other flavoproteins carry single electrons between client enzymes, alternating between the flavin's oxidized state (OX) and its anionic semiquinone (ASQ) in the case of canonical ETFs (8), or between neutral semiquinone (NSQ) and anionic hydroquinone (AHQ) in the case of flavodoxin's low reduction midpoint potential (low-*E*°) couple describing acquisition of an electron (9). The environments produced by the protein are thus crucial in shaping the redox reactivity displayed by the enzyme (9,10), as well as the flavin's spectral signatures(11-13).

In bifurcating ETFs (Bf-ETFs) the ET-FAD is analogous to the single FAD of canonical ETFs (14) and undergoes reduction by one-electron ($1e^-$) steps from OX to ASQ to fully reduced AHQ (15). The Bf-FAD unique to Bf-ETFs replaces a structural AMP present in canonical ETFs (14,16). The ET-FAD is bound in the head domain, while the Bf-FAD is bound in the base with its flavin in the interface

between the S (small) and L (large) subunits (Figure 1) (14,16). The presence of two FADs with heavily overlapped optical signals complicates studies of their individual contributions (17-19). However a combination of biochemical, spectroscopic, thermodynamic and computational tests established the above roles and reactivities of the individual flavins (16), confirming homology-based models (14) and elegant demonstration of the direction of electron transfer (18).

In contrast to the ET-FAD, the Bf-FAD's semiquinone state is thermodynamically unstable, enabling this flavin to reduce carriers with $E°$'s below the flavin two-electron ($2e^-$) $E°$, so long as an oxidant able to 'pay for' generation of the transient semiquinone is present (20,21). This latter role is played by the ET-FAD. Thus, the Bf-FAD accepts pairs of electrons from NADH ($E°'_{NADH}$ = -320 mV), sends one electron and most of the energy to a low-$E°$ ferredoxin or the NSQ/HQ couple of flavodoxin ($E°' \leq$ -400 mV (22-24)), whereas transfer of the other electron to a high-$E°$ acceptor (25,26) renders the overall reaction favorable (21,26-29). Thus the system trades quantity for quality, producing low-$E°$ electrons able to drive energetically demanding reactions such as nitrogen fixation, although NADH cannot (27,30).

The presence of two FADs may also be responsible for another feature present in *Rpa*ETF but not canonical ETFs. An absorbance band at 726 nm grows as the ET-FAD is reduced but diminishes as the Bf-FAD is reduced, suggesting that it originates from interaction between reduced ET-FAD and oxidized Bf-FAD, or between the two FADs in their semiquinone states (19). Signals in this spectral region commonly arise from charge transfer (CT) species involving a flavin and a substrate or product (31-38). However, formation of the 726 nm band was shown to be independent of the identity of the electron donor, making it intrinsic to the ETF (19). The possibility of a flavin triplet seems unlikely given the longevity of this signal (39).

Herein we report progress in elucidating the origin and nature of this intriguing species, focusing on the two FADs and their binding sites (Figure 1). We found that each of the two FADs is required for formation of the 726 nm band. Similarly, mutations affecting either binding site were found to affect the amplitude with which the 726 nm band is formed. Consistent with studies on free FMN in solution (32,40), we also present evidence that the proposed complex of two FADs responsible for the 726 nm band ('726 nm species' henceforth) possesses inherent stability, as it survives even as protection provided by the protein structure is weakened.

Given the well-documented greater-than 80° rotation of the ETF head domain (41-45) and its effect of moving the surface-exposed ET-FAD relative to the Bf-FAD, we suggest that the 726 nm band reflects further rotation of the head domain that places the ET-flavin in contact with the Bf-flavin. We note the possible significance to electron transfer of direct flavin-flavin contact, especially in the context of the gating role that has been proposed for head domain rotation (14,45).

Results

Formation and Reversibility – When wild-type (WT) *Rpa*ETF was reduced stepwise using dithionite or the xanthine and xanthine oxidase system (46) the 726 nm band grew to maximum amplitude half-way through the titration and then decreased again (Figure 2A). Qualitatively similar behavior was observed with NADH as the reductant, although maximization and decay of the signal occurred at somewhat higher NADH concentrations suggesting that stoichiometric additions of NADH do not fall in the tight-binding regime (see below). However the 726 nm species itself does not appear to be a transient intermediate as it was stable over days under inert atmosphere. The band is seen to extend to long wavelengths as for other flavin CT bands, but it displays apparent structure (Figure 2B). While vibrational structure is evident in absorption bands of individual flavins it is generally not observable on the broader supramolecular CT transitions (47). We speculate that the protein environment may suppress movement of one partner relative to the other that might otherwise be associated with the transition.

The 726 nm band could also be formed in oxidative titrations (Figure 2C). When NAD^+ was used to oxidize *Rpa*ETF that had been fully reduced by prior treatment with dithionite, the CT band at 726 nm grew initially, concurrent with appearance of spectral features of OX flavin (Figure 2C). Upon addition of excess NAD^+ it was even possible to decrease the amount of 726 nm species present as more flavin was converted to OX (below). Therefore the 726 nm species represents a state function rather than an intermediate of a particular path.

Sensitivity to pH – The 726 nm band appeared at 726 ± 2 nm at pH 8 and pH 9,

however the amplitude of the 726 nm band was 4.5-fold larger at pH 9, in titrations with NADH. Thus it does not appear to reflect the conjugate acid of an acid/base equilibrium and we rule out the NSQ state of a flavin, although that of 8-formyl flavin can absorb in this range (48) (but see (49)). Thus, although the use of pH 9 incurs the risk of increased 8-formyl flavin formation (48), we used pH 9 to optimize our ability to detect and quantify the 726 nm signal to elucidate the nature of the species responsible. Other work underway is testing a possible relationship between formation of the 726 nm species and accumulation of modified flavin, because the latter is also favoured by higher pH and correlated with a particular conformation of the ETF (48) (supporting Figure S1). The higher 726 nm species yield at high pH suggests that the 726 nm species is favored by deprotonation of an amino acid side chain nearby, or equivalently that another state in equilibrium with the 726 nm species is disfavored by the amino acid's deprotonation. To identify candidate amino acids, one must know where the 726 nm species resides.

Absence of either ET-FAD or Bf-FAD abolishes the 726 nm band – In our previous studies, we showed that the 726 nm species correlates with the oxidation states of both ET-FAD and Bf-FAD (19). We therefore proposed a delocalized CT involving both flavins (50). Consistent with this, a *Rpa*ETF variant retaining the ET-FAD but lacking Bf-FAD was found to not form the 726 nm band (16), even at pH 9. In that variant, the ET-FAD retained WT-like behavior including the same succession of two $1e^-$ reductions via an ASQ intermediate, as well as $E°$s and spectra similar to those of WT *Rpa*ETF. Because the reactivity of the ET-FAD was not greatly altered, perturbation of the ET-flavin could not explain the absence of 726 nm band from this variant. Instead, we propose that loss of the 726 nm band was due to the absence of Bf-FAD.

To test for a similar requirement for ET-FAD, we exploited the facts that 1) the ET-FAD binds with a lower affinity than does the Bf-FAD of Bf-ETFs and 2) binding is predominantly via the ADP moiety, rather than the FMN component of FAD (14,17,51,52). Therefore we used ADP to displace *Rpa*ETF's ET-FAD, to produce *Rpa*ETF containing only the Bf-flavin.

*Rpa*ETF was titrated with concentrated ADP solution while monitoring the absorbance at 400 nm (17), (Figure 3A). Once the shape of the absorption spectrum ceased to change, we inferred that remaining FAD was more resistant to displacement and therefore mostly in the Bf site. This *Rpa*ETF retained ET-FAD in 24% of sites based on the amplitude of ASQ that could be formed. Upon titration with dithionite, ET-FAD-depleted *Rpa*ETF formed much less of the 726 nm species than did WT *Rpa*ETF (compare Figure 3B with 2A). The small amount produced was attributable to the fraction of ET sites retaining FAD even after treatment.

Interestingly, the resting state enzyme prior to treatment with ADP contained a discernable amount of the 726 nm species (Figure 3A, red curve). This seemed more resistant to ADP competition than the population with both flavins OX, possibly reflecting a conformational difference. However this residual 726 nm signal decreased as the sample was reduced, and additional 726 nm intensity was not formed from the OX FAD present, in contrast with the untreated case (Figure 2A). Thus absence of ET-FAD prevents formation of the 726 nm band.

At the endpoint of reduction (in excess dithionite) ET-FAD-depleted *Rpa*ETF displayed a species resistant to further reduction (magenta spectrum in Figure 3B). Since free FAD has a higher reduction midpoint potential than that of Bf-FAD (19), we expect it to be fully reduced, and propose instead that the recalcitrant species corresponds to bound FAD. To test the possibility that a two-electron donor is required, we employed NADH under the same conditions, with the same result.

In case ET-FAD is involved in forming the 726 nm species, but is not a component of the species, we first generated a maximal amount of 726 nm species via titration with dithionite and *then* displaced ET-FAD using ADP (Figure 4A). Most of the FAD that remained bound occupied the Bf site, based on the previously-assigned CD signatures of Bf-FAD and ET-FAD (16,19) (Figure 4B), and deconvolution of the observed CD spectrum indicated that only 26% of ET sites retained FAD.

Displacement of ET-FAD from half-reduced *Rpa*ETF was accompanied by drastic diminution of the 726 nm band to only 26% of its previous intensity, demonstrating a requirement for the ET-FAD even for retention of pre-formed 726 nm band. The surviving small population retaining the 726 nm band underwent $2e^-$ reduction to HQ when additional dithionite was added, confirming the presence of Bf-FAD (Figure 4C). Increased signal from OX as well as HQ FAD was observed as ADP was added (456 and 320 nm, Figure 4A). Thus, we propose that

disruption of the 726 nm species and attendant supramolecular orbitals restores population and transition moment amplitude to the electronic transitions that characterize monomeric flavins. Indeed, this replicates in reverse the diminution of band intensity between 300 and 500 nm observed in conjunction with CT band formation when old yellow enzyme was titrated with *p*-chlorophenol (31), strengthening our assignment of the 726 nm band to a CT complex.

Thus, regardless of whether ET-FAD is displaced before or after formation of the 726 nm species, its displacement eliminates the 726 nm species. We conclude that the ET-flavin and the Bf-flavin are both indispensable for the 726 nm species.

Identities of the flavin oxidation states – Difference spectra were calculated to reveal spectral changes associated with formation and then disappearance of the 726 nm band in a dithionite titration of WT *Rpa*ETF (Figure 5). In difference spectra depicting spectral changes vs. the starting spectrum of *Rpa*ETF containing OX ET-FAD and OX-Bf-FAD (ET_{OX}/Bf_{OX}), maximal 726 nm amplitude correlated less well with initial conversion of OX flavin to ASQ (gained amplitude near 374 nm with little net change near 456 nm, Figures 5B and C) but correlated well with subsequent consumption of ASQ to form HQ (lost amplitude near 374 nm, and 510 nm which is almost isosbestic for conversion of OX to ASQ but loses intensity as ASQ is converted to HQ, Figure 5C). Difference spectra for the second half of the titration, in which the 726 nm species undergoes reduction, showed loss of that species to be accompanied by reduction of an OX flavin to HQ (456 and 374 nm, the Bf-FAD, Figure 5D). Thus, optical spectra indicate that ET-FAD_{HQ} and Bf-FAD_{OX} are present when the 726 nm band has maximum amplitude in WT *Rpa*ETF. We therefore propose that the 726 nm species could be a $flavin_{OX}$•$flavin_{HQ}$ CT complex, specifically ET_{HQ}•Bf_{OX}.

At maximum, approximately 65% of sites formed the 726 nm species, based on a plot of its amplitude vs. absorbance at 378 nm. (supporting Figure S2). This value is similar to the prediction of 80% obtained based on the *E*°s associated with the redox equilibria by which the ET_{HQ}/Bf_{OX} state is formed and consumed.

Replacements of Tyr37.S: delocalized charge transfer between ET-FAD and Bf-FAD or conformational effect? – Situated about 4 Å away from the ET-FAD and 15 Å from the Bf-FAD (14), the conserved Tyr at position 37 is an attractive candidate to facilitate electron hopping between the flavins (53,54) or delocalized CT (50), since the flavins are 18 Å apart in the B-like conformation of Bf-ETF that has been captured crystallographically (Figure 1B (45)). Because long-range electron transfer has been observed via Tyr and Trp, but is considered negligible via Phe (53) we tested for a requirement for Tyr or Trp at position 37 for formation of the 726 nm species.

The Y37F.S variant formed little if any of the 726 nm band during reduction by NADH (Figure 6A). Instead, we observed a broad and weak CT band extending from 620 nm to beyond 800 nm (Figure 6A). At least two such bands were detected in the Bf-ETF from *Pyrobaculum aerophilum* upon reduction using NADH or upon addition of NAD^+ to reduced material (15). Since NADH and presumably NAD^+ bind at the Bf-FAD site (14,16,18), these broad CT bands likely reflect Bf-FAD_{HQ}•NAD^+ complexes, in more than one conformation (15). Indeed, no such band was formed when the reductant was dithionite (supporting Figure S3). The finding that Y37F.S *Rpa*ETF forms hardly any 726 nm species also argues against the signal being due to an impurity co-purifying or bound to the ETF, as it is all but eliminated by this one amino acid substitution.

Y37W.S *Rpa*ETF accumulated a low yield of 726 nm band that can be largely explained by low FAD content (Figure 6B, and caption). After accounting for a flavin stoichiometry of only 1.2 per ETF dimer (supporting Table S1), the 726 nm band was not stronger than that of WT, although the side chain *E*° of Trp is considered as well or better able to mediate hole hopping than Tyr (53). This argues against efficient hole hopping via residue 37. If the side chain of Tyr37.S participates in long-range CT, the band might also be expected to occur at a different wavelength in the Y37W variant (for example, see (55)). Instead, Y37W.S *Rpa*ETF yielded a signal at 726 ±2 nm. Therefore, the diminished intensity likely stems from other causes. The impaired FAD binding to the Y37W.S variant suggests that the added bulk of the Trp side chain perturbs the flavin binding site(s) and could similarly affect the stability of the conformation corresponding to the proposed 726 nm species.

Y37F.S *Rpa*ETF's lack of 726 nm band can be understood on the same basis. In contrast to Y37W.S, Y37F.S was notably *more* stable than WT, in the ET_{OX}/Bf_{OX} state. Thus effects of amino acid substitution at position 37 appear to

extend beyond the ET-FAD_{HQ}/Bf-FAD_{OX} state in which CT could occur, and the absence of 726 nm band from Y37F.S could stem from global protein conformational effects rather than residue-specific ones such as residue $E°$. Thus, considering the 15 Å distance between residue 37 and the Bf-flavin, as well as residue 37's position at the interface between domains, it seems most likely that the effects of substitution at position 37 are the result of conformational effects. We favor the interpretation that altered bulk at position 37 modulates the stability of conformations that compete against the one responsible for the 726 nm band, thus changing its population without changing its nature.

Substitution of Cys174.L makes the 726 nm complex resistant to reaction with NADH/NAD^+ – The Bf site is devoid of aromatic amino acids, but electron-rich Cys and Met are in-principle also able to act as CT donors to oxidized flavins (53,56), and Cys174.L is situated adjacent to the flavin C6 of Bf-flavin (Figure 1). It is conserved among Bf-ETFs from diazotrophic bacteria such as *R. palustris*, *Azotobacter vinelandii* and *Rhodospirillum rubrum* (57) but is replaced by Ala in most non-diazotrophic Bf-ETFs, implying that it is not essential for electron bifurcation but could play a role related to diazotrophy. The greater strength of the 726 nm band at pH 9 than at pH 8 raised the possibility that ionization of Cys174.L is involved in the 726 nm band. We tested this by replacing Cys174.L with alanine.

C174A.L *Rpa*ETF retained full flavin occupancy comparable to WT (supporting Table S1) and likewise produced maximal amplitude of the 726 nm band when the protein was half-reduced by dithionite, but with nearly three-fold lower maximum yield (Figure 7A vs. 2A).

The lower yield of 726 nm complex in C174A.L could result from elevation of the Bf-FAD's $E°_{OX/HQ}$ because more favorable reduction of the Bf-flavin would diminish the extent to which Bf-FAD_{OX} co-exists with ET-FAD_{HQ}. Redox titrations revealed that the $E°'_{OX/HQ}$ of the Bf-FAD is -216 ±5 mV (n=3) (vs. -223 mV for WT, both calculated based on values measured at pH 9 (19)), supporting Figure S4). This small of an effect is surprising given that at pH=9 Cys174.L is predicted to be anionic, and flavin reduction is predicted to yield anionic AHQ, so we would anticipate relief from an electrostatic impediment to reduction, in C174A.L. Further tests are required to determine whether the Bf-FAD (together with Cys174.L) takes up two protons upon $2e^-$ reduction, making the reduction electrostatically neutral. However we note that the 726 nm band was stronger at pH 9 than at pH 8 even for C174A.L *Rpa*ETF, demonstrating that ionization of Cys174.L is not the basis for the pH effect.

Although less likely to respond to replacement of C174.L, the $E°'_{ASQ/HQ}$ of the ET-FAD could also affect yield of 726 nm species. The results of two independent titrations yielded $E°'$= -90 mV for the ASQ/HQ couple of the ET-flavin in C174A.L, *vs*. a value of -83 mV for WT (19) (supporting Figure S5). The two small shifts in $E°$ conspire to predict a 7% decrease in yield of 726 nm species in C174A.L assuming the 726 nm species involves the HQ state of ET-flavin and the OX state of Bf-flavin (supporting Figure S6B). This fails to account for the three-fold diminution observed, indicating that factors additional to the flavin $E°$s contribute to the lower 726 nm species yield in C174A.L vs. WT *Rpa*ETF.

When the physiological electron donor NADH was employed to reduce C174A.L *Rpa*ETF, the 726 nm band did not diminish towards the end of the titration in the usual NADH concentration range (Figure 7B vs. 7A, and 6C). C174A.L's recalcitrance could reflect lower reactivity with NADH as the C174A.L *Rpa*ETF also accumulated less ASQ early in the titration, similar to what has also been observed among canonical ETFs (58). When electrons were supplied using dithionite or xanthine/xanthine oxidase via a mediator, more ASQ formed and the 726 nm band diminished as the system became fully reduced (supporting Figure S4). Thus C174A.L *Rpa*ETF's impeded reaction with NADH appears to be particular to this reductant.

To test whether C174A.L's 726 nm species was resistant to reduction in particular, we tested its formation and decay in oxidative titrations. Figures 8A and B show that the 726 nm species has the status of an intermediate that formed and then declined in the course of oxidative titrations of WT *Rpa*ETF with NAD^+, as in reductive titrations. C174A.L that had been fully reduced by dithionite also formed the 726 nm species upon oxidation with NAD^+ (Figure 8C). As for WT, the signature of OX flavin was seen to grow in tandem with that of the 726 nm species, consistent with participation of Bf-FAD_{OX}. However a much higher concentration of NAD^+ was required to form the 726 nm species starting from fully reduced C174A.L than for WT (Figure 8D, note different horizontal axes). Similarly, prominent accumulation of NADH was observed in the presence of reduced

C174A.L (panel C, near 340 nm). This could reflect excess dithionite present as required to fully reduce the C174A.L *Rpa*ETF to start with, and then ETF-catalyzed reduction of added NAD^+ by the excess dithionite. Given that both reduction of C174A.L *Rpa*ETF by NADH and its oxidation by NAD^+ required higher concentrations of the nicotinamide, and given that the flavin $E°$ in effect was not very different from that of WT, we conclude that C174A.L *Rpa*ETF has a diminished affinity for NADH/NAD^+.

As the physiological substrate, NADH may be more than simply an electron donor, as its binding, or release of NAD^+, could be coupled to reorientation of ETF's head domain (14). Demmer *et al* found that the NADH-binding site is obstructed in the D conformation of *Cdi*ETF. Thus it may be that substitution of Ala for C174.L favors the D conformation especially when ET-FAD is reduced. If so, the lowered maximal yields of 726 nm species in C174A.L suggest that the 726 nm species corresponds to a conformation other than D. Regardless, the finding that the 726 nm species of C174A.L *Rpa*ETF resists further reduction with NADH provides a convenient means of accumulating it for detailed study.

The 726 nm complex persists even as protein tertiary structure dissolves – Studies of FMN in aqueous solution document formation of change-transfer dimers of FMN_{HQ}•FMN_{OX} and demonstrate that the association between a FMN_{HQ} and a FMN_{OX} is inherently favorable ((40) and supporting Figure S7). Therefore, if the 726 nm complex corresponds to a $flavin_{HQ}$•$flavin_{OX}$ association, it should persist (temporarily) if protein structure around it is compromised.

To dissolve protein structure without forming precipitate, we adopted the method of Gross *et al* (59) wherein cetyltrimethylammonium bromide (CTAB, a cationic surfactant) presumably loosens the protein tertiary structure but does not produce protein precipitation. Indeed, even after heating to 100 °C, *Rpa*ETF displayed no aggregation in the presence of 10 mM CTAB. Near-UV CD reflecting Trp side chains in anisotropic ordered environments (60) decayed with a half-time of only 3 minutes upon addition of CTAB (Figure 9B). However absorbance at 726 nm diminished with a half-time of approximately 37 minutes (Figure 9A).

Even before addition of CTAB, the flavin fluorescence of ET_{HQ}/Bf_{OX} *Rpa*ETF was already greatly quenched compared to that of fully oxidized (ET_{OX}/Bf_{OX}) *Rpa*ETF, consistent with CT character in the 726 nm state (61,62) (black vs. grey curves in Figure 9C). However in the course of an hour's incubation in CTAB, flavin fluorescence intensity dropped further suggesting increased quenching, presumably by the attached adenine upon FAD dissociation (63,64). Since heating in air produced little additional effect, it appears that the effect was almost complete after an hour in CTAB.

Trp fluorescence was almost fully unmasked by an hour's treatment with CTAB (Figure 9D). For the flavins as well as the Trps, fluorescence emission maxima shifted to longer wavelengths consistent with greater exposure to polar solvent (65). Thus, global signatures of protein tertiary structure indicated that the core of *Rpa*ETF was no longer packed in a unique long-lived structure, but became less ordered and extensively hydrated in the course of an hour's incubation with CTAB. (Also see supporting Figure S8.) Despite the almost complete loss of protein structural integrity, the 726 nm band retained almost half of its amplitude over the same time interval.

The 726 nm species nonetheless represents a non-covalent association dependent on flavin oxidation states, as exposure to air and heating to boiling temperature for 10 minutes abolished the signal.

Hence it appears that the 726 nm species persists longer than protein tertiary structure in general, suggesting that the proposed ET-$flavin_{HQ}$• Bf-$flavin_{OX}$ complex is inherently stable or resides in a portion or conformation of the protein that is particularly resistant to unfolding. Specific interactions between the proposed 726 nm complex and protein residues may persist on the same time scale as the signal, as indicated by the invariance of the wavelength and line width.

As an inherently stable entity, the proposed $flavin_{HQ}$•$flavin_{OX}$ CT complex should survive computational geometry optimization without any protein ligands to constrain the flavins to stay together. We tested this using density functional theoretical energy minimization with two different functionals in conjunction with two different basis sets, and two geometries of flavin dimers, drawn from the crystal structures of dodecins (66,67). One of the flavins (modeled by lumiflavin) was modeled in the neutral HQ state and the other as OX, in each pair. All four calculations arrived at stable energy minima. Calculated optical spectra for individual OX and

HQ lumiflavins reproduced the dominant features observed for FMN (Figure 10). The natures of the orbitals and the transitions observed could be related to those seen in isolated flavin$_{OX}$ *or* flavin$_{HQ}$ monomers, with the exception that all four calculations of dimers predicted a new long-wavelength band (Figure 10 and supporting Figures S9 and S10). The strength of the band and its transition energy (wavelength) varied with the computational methodology and flavin dimer geometry, likely because the different methods and starting structures produced distinct stacking and angles between the flavins (supporting Figure S9) (68). A control calculation in which both flavins were OX did not minimize to a π-stacked geometry. However the flavin$_{HQ}$•flavin$_{OX}$ dimers were all stable despite the absence of any hydrogen bonding partners to mediate interactions between them. Finally, the calculated displacements of electron density associated with the new long-wavelength bands all confirmed that they were CT bands by nature, associated with electron density migration from the HQ to the OX flavin (Figures 10, S9). This confirms that a π stacked flavin$_{HQ}$•flavin$_{OX}$ complex is in-principle a viable proposal compatible with the optical signature observed, provided that protein movements permit it.

Discussion

We report a work in progress, as this story appears to involve additional variables such as pH, possible correlation with flavin modification, and factors that may modulate the orientation of the head domain relative to the base. However we present evidence that the 726 nm band involves participation by both the flavins of *Rpa*ETF, apparently as ET-FAD$_{HQ}$ and Bf-FAD$_{OX}$. The Y37F.S, Y37W.S and C174A.L substitutions that affect 726 nm yield can each act via multiple mechanisms, but a unifying hypothesis is that they alter the relative stability of an orientation of the head domain that places the two flavins in van der Waals contact with one-another. The resolved features of the 726 nm band (compared to conventional CT bands) suggests that the proposed flavin$_{HQ}$ to flavin$_{OX}$ transition is associated very little reorganization within the complex (69) and see for example (70). This is consistent with the proposed 726 nm CT complex being coupled to the much larger inertias of protein domains.

A corollary of our proposal of van der Waals contact between the two flavins is that the 'B-like' conformation captured crystallographically does not represent the full extent to which the head domain can rotate. The latter has already been proposed by the original authors and was the basis for their 'B-like' terminology rather than simply 'B', because they postulated a greater amplitude of rotation in solution, resulting in a flavin-flavin distance of 14 Å rather than the 18 Å captured in the crystal structure (14). Likewise, we note that relatively undemanding side chain and loop movements suffice to allow the head domain orientation to be further rotated bringing the flavins closer together. Building on the earlier work, we present the first evidence to our knowledge that the two flavins may come in contact.

Our proposal of a CT complex between the flavins themselves is consistent with the lack of significant wavelength shift or linewidth change upon substituting nearby Cys, Tyr or Trp that are known to be able to engage in CT with flavins (62,71,72). CT bands between flavins and stacked aromatic groups generally apply to OX flavin and manifest as absorbance extending to longer wavelengths than the 500 nm cutoff typifying OX flavin alone (73,74). They are understood to result from orbital overlap producing hybrid orbitals with supramolecular character (36,75). Participation of Tyr37.S in the 726 nm complex is unlikely because Tyr or Trp are expected to act as CT donors to an OX flavin whereas our titrations in Figure 5 demonstrate that the flavin near Y37.S adopts the HQ state in the 726 nm species (the ET-flavin, Figure 1). Meanwhile the Bf-flavin is not mobile relative to residue 37 and is 12 Å away from the nearest aromatic side chain based on our model and available structures (14). Cys is competent to form a CT complex with OX Bf-flavin, especially upon ionization (76,77). However C174.L was proven not to be required for 726 nm species formation by our C174A.L variant. These findings corroborate the lack of wavelength change, arguing against inclusion of C174.L or Y37.S in the CT species. Thus the simplest proposal consistent with the data in hand at present is that the 726 nm species is comprised of ET$_{HQ}$•Bf$_{OX}$.

Although our proposal is novel in the context of ETFs, ample structural precedent for π-stacked flavin dimers is provided by the dodecins. Bacterial dodecin from *Thermus thermophilus* displays pairs of *si-si* stacked flavins whereas *re-re* stacked pairs are observed in *Halobacterium salinarum* dodecin (66,67). Interestingly, dodecins extend the π-stack by contributing Trp side chains that flank the flavin dimer on either side to generate a 4-layer stack.

Absorbance extends to wavelengths longer than 500 nm (66,67) as in the Tyr/flavin/Trp stack of flavodoxin (71,78) and riboflavin-binding protein (79). In an elegant study wherein Trp analogs varying with respect to electron donating ability were installed in dodecin in place of the stacked Trp, analogs with lower tendency to donate electron density showed less long-wavelength absorbance whereas presence of the better electron donor 4-NH_2-Trp resulted in a resolved CT band centred near 670 nm, and accelerated electron transfer to photoexcited flavin (55).

Dodecins are believed to prevent photodamage catalyzed by flavins by passivating the flavin's intrinsic photoreactivity (80). The binding mode allows retention of the OX flavin's absorbance spectrum but essentially abolishes fluorescence and triplet formation due to very rapid electron transfer from the stacked Trp that outcompetes other events (55,62,67). Similarly rapid electron transfer between two flavins is expected if one were present as the HQ, as we propose here.

Thermodynamic and optical spectroscopic data document binding of flavin dimers in flavodoxin (81), and one of the most celebrated structures in molecular biology, that of B-form DNA, reveals that π stacking among DNA bases provides the structural basis for the stability of the hydrophobic core of DNA (82). These examples demonstrate the plausibility of stacking among flavins.

The inherent favourability of such an interaction is demonstrated by the fact that riboflavin and FMN dimerize with a K_d of approximately 10 mM for OX/OX dimers or HQ/HQ dimers that can be substantially attributed to the hydrophobic effect since it is unique to aqueous solutions (40) and dimerization is suppressed above room temperature (83). This is consistent with model studies and computation indicating that π-stacked OX/OX flavin dimers are stabilized by approximately 2 kJ/mol (84,85) reflecting dispersion interaction between the participating π systems (68,86) and hydrogen bonding (68,83). OX/OX π-stacked dimers display a diagnostic shoulder at 485 nm and long wavelength absorption extending beyond 550 nm (87,88).

When one of the two flavins is reduced to the HQ state, additional dipolar stabilization produces a K_d of 0.5 mM (40). Such OX/HQ dimers are presumably at equilibrium with flavin SQs, monomers or dimers (89). However EPR and UV/visible spectral signatures argue that in half-reduced solutions with flavin concentrations above 2 mM, the dominant species is the OX/HQ dimer (32,40,90). This is consistent with the $E°$s of free flavin that favour disproportionation of SQ, which is populated to a maximum of only 1% in dilute solution at half-reduction (3,91). The flavin HQ/OX complex CT absorption maximum varies in the range of 770 - 1100 depending on the pH, and presence of additives (40,89). Considering that Bf-ETFs constrain two flavins to be within 41 Å of one another (D conformation) which constitutes an effective concentration of 6 mM, we should not be surprized if the flavins were to dimerize, in competition with other equally favourable interactions.

The natural proclivity of flavins to form dimers could also cause otherwise short-lived or infrequent states to be captured when concentrations are high. π-stacked flavin dimers have been directly observed in structures resulting from crystals soaked in 23 mM FMN (92), 1 mM FMN (93) or grown from 0.5 mM enzyme in a 0.5 mM solution of FMN (94). In these latter cases, the mechanisms of the enzymes in question allow that the flavin dimers observed may reflect *bona-fide* catalytic intermediates.

The EmoB crystal structure shows a *si-si* stack of two flavins, with a Tyr side chain below the tightly bound one (93). EmoB is a flavin reductase proposed to accept hydride from NADH in a reductive half-reaction, and then pass it to FMN substrate in an oxidative half reaction that would involve a flavin-to-flavin hydride transfer facilitated by stacking of the two flavins (93). In dihydromethanopterin reductase (DmrB), a weakly-bound FMN is resolved stacked against the tightly bound FMN to form a *re-re* π stacked dimer. (94). Here too, the enzyme is proposed to employ tightly-bound FMN to reduce a substrate FMN that binds via a transient stacked conformation (94).

In EmoB and DmrB, it appears that both flavins were OX, and long wavelength spectra were not shown in either case. However given that the tightly bound FMNs are both proposed to alternate between OX and HQ states, and the substrate FMN is proposed to bind as OX when the tightly-bound FMN is HQ, we expect that the E•S and E•P intermediates should represent π-stacked OX/HQ, as we propose for *Rpa*ETF. Based on our work, we predict that if the oxidative reactions of EmoB or DmrB can be observed at long wavelengths with sufficiently

short dead-times they will display transient $flavin_{HQ}$•$flavin_{OX}$ CT bands.

In our case we do not think that we form a π-stacked dimer in a single one of the two binding sites. The flavin stoichiometry of our preparations is close to 2 per ETF heterodimer and the flavins have distinct *E*°s different from those of free flavin indicating that the two flavins occupy different binding sites. Moreover amino acid substitutions in either binding site decreased the yield of the 726 nm species indicating that both protein sites contribute to its population. Thus we hypothesize that the two sites are allowed come together by head domain movement, and that favourable flavin•flavin interaction stabilizes this conformation (40).

Structural and computational studies are required to flesh out a proposal for a protein conformation compatible with van der Waals contact between the two flavins, but persistence of the 726 nm band in the course of gentle unfolding is consistent with the stability of π-stacked flavin dimers in solution (40). It demonstrates that the CT complex is not merely imposed by protein, but rather a contributor to the stability of the proposed B state.

Regarding possible mechanistic significance, a CT complex uniting the two flavins would accelerate electron transfer between them. However, the proposed extremely rapid electron transfer would be conditional on population of the B conformation, i.e. it would be conformationally gated. Any interactions that alter the relative stability of B vs. D conformations would thereby modulate the effective rate of electron transfer. Given that the D conformation has been captured only when the partner CoA dehydrogenase (analogous to FixC) was present, the foregoing suggests that FixC binding will disfavor the B conformation, in-effect creating an open circuit between the flavins. This could prevent back-transfer of electrons from the ET-flavin to the Bf-site, and thereby increase the efficiency of bifurcation.

In the forward direction, formation of the proposed π-stacked flavin dimer could transiently stabilize a semiquinone state of the Bf flavin (40), e.g. by delocalizing unpaired electron density over both flavins. Thus, the Bf-site could suppress SQ states of *monomeric* Bf-flavin as required for optimal hydride acceptance from NADH, but formation of a π-stacked dimer with the ET-flavin could 'turn on' $1e^-$ transfer for the lifetime of the complex (95). Electron transfer from the complex would oxidize the participating flavins, causing the complex to dissolve and giving it the mechanistic status of a transition state.

Events that modulate the head domain orientation would acquire control over whether or not the proposed CT transition state could form. Candidates are binding/dissociation of partner proteins (45), or binding/dissociation of $NADH/NAD^+$ (14). While such a species may be fleeting in turnover, our use of high pH and the absence of natural partner proteins may enable it to accumulate, for lack of normal electron acceptors or a proton coupled to electron transfer. Thus, our proposed conformationally-enabled π-stacked di-flavin CT complex could coordinate several requirements for energy-efficient electron bifurcation, in the heart of Bf-ETFs.

Experimental Procedures

Site-directed mutagenesis, overexpression and purification of R. palustris ETF and its variants - Generation of a construct for the expression of WT *Rpa*ETF was described elsewhere (19). The vectors pMCSG28 and pMCSG21 were acquired from DNASU Plasmid Repository (Tempe, AZ), and augmented with the genes for EtfS (also known as FixA) and EtfL (also known as FixB), respectively. The plasmids of EtfS variants Y37F.S, Y37W.S, and EtfL variant C174A.L were prepared using mutagenic primers [5'-CAATCCCTTCGATCTGTTCGCGCTCG-3' (Y37F.S coding), 5'-ATGATCGTCGGCACGCCCTGGC-3' (Y37F.S non-coding), 5'-CAATCCCTGGGATCTGTTCGCGCTCG-3' (Y37W.S coding), 5'-ATGATCGTCGGCACGCCCTGGC-3' (Y37W.S non-coding), 5'-GCTGCTGGCGACGATCTACACGC-3' (C174A.L coding), and 5'-GAGCCGCCGAAGGTCGGACG-3' (C174A.L non-coding)] according to the Q5® Site-Directed Mutagenesis Kit procedure (New England Biolabs, Ipswich, MA). After DNA sequencing verification (Eurofins Genomics, Louisville, KY), the *E. coli* strain NiCo21(DE3) (New England Biolabs, Ipswich, MA) was transformed with both plasmids for expression of desired *Rpa*ETF variants along with pGro7 (Takara Bio, Mountain View, CA) for co-expression of molecular chaperones GroES/EL. Cells were grown in 500 mL Terrific Broth supplemented with 20 mg/L riboflavin and 2 mM $MgSO_4$ along with carbenicillin (100 μg/mL), spectinomycin (100 μg/mL) and

chloramphenicol (50 µg /mL) at 37°C, shaking at 250 RPM, to an OD_{600} of ≈ 2. After fully cooling the culture to 18 °C, *groES/EL* gene expression was induced with 1 mg/mL L-arabinose. After 30 min growth, ETF gene expression was induced with 0.1 mM IPTG. Cultures were then grown for 16 additional hours at 18 °C. Cells were harvested by centrifugation at 11,899 x *g*, 4 °C for 6 min and the pellet was stored at -80 °C after washing once in phosphate-buffered saline, (10 mM Na_2HPO_4, 1.8 mM KH_2PO_4, 137 mM NaCl, 2.7 mM KCl pH 7.4).

Frozen cell pellet was thawed and resuspended in 25 mL BugBuster (EMD Millipore, Burlington, MA) containing 1 mM AEBSF (4-(2-aminoethyl)benzenesulfonyl fluoride hydrochloride), 1 mM FAD (Chem-Impex International, Wood Dale, IL), 2 µL Benzonase® Nuclease HC and 2 µL rLysozyme™ Solution (EMD Millipore, Burlington, MA), and further incubated at 4 °C for 2 hours with stirring. After centrifugation at 20,000 x *g* for 30 min at 4 °C, the supernatant was filtered through a 0.22 µm syringe filter. The resulting protein solution was mixed with 2 mL pre-equilibrated Ni-NTA resin (EMD Millipore, Burlington, MA) and incubated at 4 °C with stirring for 1 hour. Then the mixture was transferred to a column at 4 °C. After collecting the flow-through, the column was washed with 20 column volumes of 20 mM Tris, pH 7.8, 500 mM KCl containing 20 mM imidazole. Finally, the column was developed with 2 column volumes of 20 mM Tris, pH 7.8, 500 mM KCl containing 200 mM imidazole and the eluate was collected in different fractions. After SDS-PAGE analysis, imidazole was removed from the pooled pure fractions by passage over a 10DG column (Bio-Rad Laboratories, Hercules, CA) equilibrated with 20 mM bis-Tris propane, pH 9.0, 200 mM KCl, 10% (w/v) glycerol. Any apoproteins were then reconstituted by overnight incubation of the protein in 1 mM FAD at 4 °C in darkness. Excess flavin was then removed by gel filtration on a 10DG column (above) prior to prompt use or flash-freezing in liquid nitrogen and storage at -80 °C. Prior work had included TCEP in buffers as a precaution (19), but it was found to diminish yields of the 726 nm species so it was not used in the current work unless stated.

Flavin content quantification – Protein concentration was determined using the Pierce 660 nm protein assay (Thermo Fisher Scientific, Waltham, MA). No correction was found to be necessary for the use of bovine serum albumin as the standard, based on parallel protein concentration determination based on the absorbance at 280 nm of trichloroacetic acid-denatured and urea-redissolved protein (96). To quantify the flavin content, the protein sample was denatured by heating at 100 °C in the dark for 10 min. After cooling to 4 °C, the sample was centrifuged at 15,000 x *g* for 2 min to remove denatured proteins. The concentration of FAD in the supernatant was then quantified spectrophotometrically using the extinction coefficient $\varepsilon_{450} = 11.3\ mM^{-1}\ cm^{-1}$ (97).

Displacement of flavin by ADP in WT RpaETF and bound flavin identification by circular dichroism (CD) – The FAD in *Rpa*ETF with a lower binding affinity to the protein was displaced at two different oxidation states using the method of Sato et al (51). Anaerobic titrations were performed on a HP 8452A spectrophotometer (Agilent Technologies, Santa Clara, CA) equipped with an Olis controller (Bogart, GA) housed in a Belle Technology (Weymouth, United Kingdom) glovebox (<1.8 ppm of oxygen) using a 1 cm path length self-masking quartz cuvette with an airtight closed screw cap (Starna Cells, Atascadero, CA) in 20 mM bis-Tris propane, pH 9.0, 200 mM KCl, 10% (w/v) glycerol.

In the first case, 221.38 mM ADP ($\varepsilon_{260} = 15.4\ mM^{-1}\ cm^{-1}$) (98) was used to titrate 400 µL of 22.2 µM WT *Rpa*ETF until the amplitude at 400 nm ceased to change, suggesting that the majority of ET-FAD_{OX} had dissociated. Then a reductive titration of the resulting protein sample was performed using 3.32 mM sodium dithionite ($\varepsilon_{315} = 7.05\ mM^{-1}\ cm^{-1}$)(99).

In the second case, 400 µL of 68.7 µM WT *Rpa*ETF was reduced halfway by 3.42 mM sodium dithionite. Then the resulting protein sample was titrated with 637.48 mM ADP until the absorbance at 726 nm no longer changed. In order to determine which binding site retained FAD, CD spectra were recorded from 600 to 300 nm at room temperature, with the following parameters: bandwidth 2.00 nm, scanning speed 100 nm/min and accumulations 1. The molar ellipticity [θ] can be calculated using the equation: $[\theta] = \theta / (c \times l)$, in which θ is the ellipticity in mdeg, c is the concentration in millimolar, and l is the cell path length in cm. After the CD measurement, the reductive titration was resumed with sodium dithionite.

Anaerobic titration of WT, Y37F.S, Y37W.S and C174A.L RpaETF by NADH, NAD^+ and/or sodium dithionite - Anaerobic titrations were all

conducted on a HP 8452A spectrophotometer (Agilent Technologies, Santa Clara, CA) equipped with an Olis controller (Bogart, GA) housed in a Belle Technology (Weymouth, United Kingdom) glovebox (<1.8 ppm of oxygen) using a 1 cm path length self-masking quartz cuvette with an airtight closed screw cap (Starna Cells, Atascadero, CA) in 20 mM bis-Tris propane, pH 9.0, 200 mM KCl, 10% (w/v) glycerol.

WT *Rpa*ETF was titrated using 400 µL of 21.3 µM protein with 1.22 mM NADH (ε_{340} = 6.22 mM^{-1} cm^{-1}) (100). Y37F.S *Rpa*ETF was titrated using 400 µL of 29.9 µM protein with 1.50 mM NADH. Y37W.S *Rpa*ETF was titrated using 400 µL of 15.9 µM protein with 0.65 mM NADH. C174A.L *Rpa*ETF was titrated using 400 µL of 27.4 µM protein with 2.74 mM NADH. WT *Rpa*ETF was also titrated using 400 µL of 68.7 µM protein with 3.42 mM sodium dithionite (ε_{315} = 7.05 mM^{-1} cm^{-1}) (99). C174A.L *Rpa*ETF was also titrated using 400 µL of 20.0 µM protein with 2.00 mM sodium dithionite.

Oxidative titrations using NAD^+ were performed similar to the reductive titrations under inert atmosphere. It was not possible to re-oxidize with ferricyanide, due to protein precipitation, and reaction with O_2 was not employed due to its several complicating side reactions. Fully reduced (via dithionite) WT *Rpa*ETF (13.9 µM) was titrated by 2.78 mM NAD^+ first to re-form the 726 nm species until maximum population was achieved. Then the resulting protein was further titrated by 139.00 mM NAD^+ until the 726 nm band was gone. Fully reduced (via dithionite) C174A.L variant (20.0 µM) was titrated by 3 mM NAD^+ and then 150 mM NAD^+ until the 726 nm band no longer changed. All titrations were done in 20 mM bis-Tris propane, pH 9.0, 200 mM KCl, 10% (w/v) glycerol. The following equation was used to determine the dissociation constant for NAD^+ binding:

$$y = \frac{y_{max} c}{K_d + c}$$

where y_{max} is the maximum binding shown as ε_{726}, c is NAD^+ concentration and K_d is the dissociation constant.

CD and fluorescence analysis of CTAB-treated WT RpaETF 726 nm species– In order to denature *Rpa*ETF without causing precipitation, 44 µL of 115.5 mM cetyltrimethylammonium bromide (CTAB) was mixed thoroughly with 466 µL of 9.96 µM WT *Rpa*ETF displaying the 726 nm signal. Rather than maintain a sample poised half-way through a redox titration, this experiment employed 726 nm species that had formed slowly over 20 hours in anaerobic storage at 4 °C in 20 mM bis-Tris propane, pH 9.0, 200 mM KCl, 10% (w/v) glycerol inside a Belle Technology (Weymouth, United Kingdom) glovebox (<1.8 ppm of oxygen). All other experiments used material immediately after preparation or flash-frozen immediately and thawed only at the time of use.

The absorption spectra were monitored on a HP 8453 spectrophotometer (Agilent Technologies, Santa Clara, CA) using a 1 cm path length self-masking quartz cuvette with an airtight closed screw cap (Starna Cells, Atascadero, CA) at 0 min, 5 min, 10 min, 20 min, 30 min, 40 min, 50 min and 60 min time points after thorough mixing anaerobically on ice, eventually the sample was heated at 100 °C in the dark for 10 min.

The absorbance change at 726 nm over time was fit into a single phase dissociation model:

$y = y_0\, e^{-kt}$, where y_0 is the maximum amplitude at 726 nm, t is time and *k* is the decay constant.

Near-UV CD spectra were also recorded at 4 °C from 350 to 250 nm to probe protein tertiary structure with the following parameters: bandwidth 2.00 nm, scanning speed 100 nm/min and accumulations 4. The molar ellipticity [θ] can be calculated using the equation: [θ] = θ / (c x l), in which θ is the ellipticity in mdeg, c is the ETF concentration in millimolar, and l is the cell path length in cm. The molar ellipticity change at 280 nm over time was fit into a one phase association model:

$y = y_0 + (y_{max} - y_0)\left(1 - e^{-kt}\right)$,

where y_0 is the $[\theta]_{280}$ minimum, y_{max} is the $[\theta]_{280}$ plateau, t is time and *k* is the rate constant.

Similarly, far-UV CD spectra were also recorded using 3.67 µM protein at 4 °C from 250 to 200 nm to probe protein secondary structure with the following parameters: bandwidth 2.00 nm, scanning speed 100 nm/min and accumulations 4.

The mean residue ellipticity [θ] can be calculated using the equation: [θ] = (θ x10^6) / (c x l x n), in which θ is the ellipticity in mdeg, c is the concentration (mM), l is the cell path length in mm and n is the number of peptide bonds in the protein. The mean residue ellipticity change at 222 nm over time was fit into a one phase dissociation model:

$y = y_{min} + (y_0 - y_{min})\, e^{-kt}$,

where y_0 is the $[\theta]_{222}$ maximum, y_{min} is the $[\theta]_{222}$ plateau, t is time and *k* is the rate constant.

In a similar experiment in order to produce samples for fluorescence analysis, 40 µL of 115.5 mM CTAB was mixed thoroughly with 422 µL of 12.1 µM WT *Rpa*ETF. Fluorescence emission spectra of the above native WT *Rpa*ETF protein, CTAB-treated protein (after 60 min) and further heat-denatured protein were recorded using a 2 mm path length fluorescence quartz cuvette with an airtight closed screw cap (Starna Cells, Atascadero, CA) on a Thermo Scientific Lumina Fluorescence Spectrometer (Waltham, MA) with the following parameters: for tryptophan fluorescence, excitation wavelength 295 nm, emission wavelength 310-450 nm, excitation slit 2.5 nm, emission slit 1 nm, integration time 20 ms, response time 0.1 s, average number 3; for flavin fluorescence, excitation wavelength 466 nm, emission wavelength 480-720 nm, excitation slit 5 nm, emission slit 2.5 nm, integration time 20 ms, response time 0.1 s, average number 3. Note that upon flavin dissociation, flavin fluorescence becomes strongly quenched by the attached adenine (63,64).

Reduction midpoint potential determination of Bf-FAD of C174A.L RpaETF – The $E°$ (Bf-$FAD_{OX/HQ}$) of C174A.L variant was determined using the xanthine/xanthine oxidase method as described previously (19) using phenosafranin as the mediator-cum-redox buffer and sensor. Linear regression analysis of $\ln([FAD_{OX}]/[FAD_{RED}])$ vs. $\ln([Dye_{OX}]/[Dye_{RED}])$ was performed using GraphPad Prism version 8.2.1 for Mac OS X (GraphPad Software, La Jolla, CA) and fit into the following equation:

$$ln\left(\frac{[F_{OX}]}{[F_{RED}]}\right) = b + \frac{n_F}{n_D} ln\left(\frac{[D_{OX}]}{[D_{RED}]}\right)$$

where $[F_{OX}]$ is the concentration of the reacting flavin in the oxidized state, $[F_{RED}]$ is the concentration in the state formed upon reduction, $[D_{OX}]$ and $[D_{RED}]$ have the same meanings for the dye, n_F and n_D denote the number of electrons acquired by the flavin and the dye, respectively, in the reaction under study, and b is the intercept produced by the fit. The value obtained for b was then used with the midpoint potential of the dye, $E°_D$, to calculate that of the flavin, $E°_F$, using the following equation:

$$b = \frac{n_F}{25.7\ mV}(E_D^0 - E_F^0)$$

where 25.7 mV replaces *RT/F* (ideal gas constant times absolute temperature divided by Faraday's constant). For phenosafranin, n = 2 and $E°_D$ = -252 mV at pH 7, which was adjusted to -312 mV at pH 9 based on phenosafranin's uptake of one proton per 2 electrons between pH 7 and 9. For Nile blue, n = 2 and $E°_D$ = -116 mV at pH 7, which was adjusted to -176 mV at pH 9 based on Nile blue's uptake of one proton per 2 electrons between pH 7 and 9.

Computations – Density functional theory (DFT) calculations were performed using Gaussian 16 (101). Starting geometries for flavin dimers were drawn from the crystal structures of dodecins. Coordinates for a *re* face to *re* face dimer were extracted from *Halobacterium salinarum* dodecin (2CCC.pdb (66)), and a *si-si* dimer was extracted from the coordinates of *Thermus thermophilus* dodecin (2V18.pdb (67)). Ribityl chains were truncated to methyl groups yielding lumiflavin dimers. Hydrogen atoms were added to N5 and N1 of one of the two lumiflavins to create a model for the HQ state, whereas the other lumiflavin was left as OX.

In order to test the sufficiency of the flavins themselves for formation of CT dimers, the systems were kept as simple as possible, using the polarizable continuum model for water (102). To control for possible effects of the methodology, we compared two functionals: the long-range corrected hybrid exchange-correlation functional cam-B3LYP (103) and another range-separated functional that was found to perform well in TD-DFT calculations on flavins (104): ωB97X-D (105). We also varied the basis set used in order to test whether results were general. the correlation-consistent double-zeta basis cc-pVDZ (106) was used with the cam-B3LYP functional as in (68), whereas the 6-31+G(d, p) basis (107) was used with the ωB97X-D functional as in (86).

After geometry optimization and checking for imaginary vibrations, time-dependent DFT calculations were performed to identify singlet - singlet transitions with significant strength. The computed excitation energies and oscillator strengths were used to calculate optical spectra for comparison with experimental data. TD-DFT derived vertical transition energies were too high by ≈ 0.55 eV, consistent with other work (16,108). However this does not interfere with our objective of comparing the features produced by individual flavins with those produced by CT dimers. The TD-DFT method is not ideal for transitions with a large amount of CT character (109) but its failure to treat the electrostatic attraction between CT partners is rectified substantially by use of the cam-B3LYP or ωB97X-D functionals (104), so the current qualitative comparisons can be made, with a single industry-standard approach that has an extensive track record for flavins (16,68,104).

Transition energies and amplitudes from the computations were used to calculate absorption spectra with Gaussian lines 0.5 eV wide at half height for transitions with energies up to σ = 5 eV (λ ≥ 250 nm). Individual bands were calculated using

$$\varepsilon_i(\sigma) = \frac{e^2 N\sqrt{\pi}}{10^3\ ln(10)\ c^2 m_e}\frac{f_i}{\Delta\sigma}e^{-\left\{\frac{\sigma-\sigma_i}{\Delta\sigma}\right\}^2}$$

where σ_i is the energy of the i^{th} transition in eV, f_i is the oscillator strength of the i^{th} transition, *N, c, m_e* have their usual meanings and $\varepsilon_1(\sigma)$ is the obtained extinction coefficient due to the i^{th} transition as a function of photon energy σ (110). Plots of total ε vs. wavelength were obtained by summing the contributions from all transitions with oscillator strengths ≥ 1% of the maximum value obtained for that calculation, and converting transition energies to wavelengths using λ= hc/σ where h is Planck's constant.

Molecular graphics were produced in PYMOL(111) or Chimera (112) and electron density displacement maps were generated using Gausview 06 at an isovalue of 0.0004 (113).

Data Availability

Data are contained in the manuscript as well as the supporting materials available on line in the form of 1 Table and 10 Figures. The authors welcome collegial communications on any and all content in this manuscript.

Acknowledgements

This work was supported by the National Sciences Foundation, Chemistry of Life Processes CHE-1808433. We acknowledge Prof. R. Stanley and C. Van Galen for valuable discussions, and T. Cassel and Prof. R. Higashi for challenging ICP-MS measurements.

The authors declare that they have no conflicts of interest with the contents of this article.

References

1. Massey, V. (2000) The chemical and biochemical versatility of riboflavin. *Biochem. Soc. Trans.* **28**, 283-296
2. Mansoorabadi, S. O., Thibodeaux, C. J., and Liu, H. W. (2007) The diverse roles of flavin coenzymes–nature's most versatile thespians. *J. Org. Chem.* **72**, 6329-6342
3. Mayhew, S. G. (1999) The Effects of pH and Semiquinone Formation on the Oxidation-Reduction Potentials of Flavin Mononucleotide: A Reappraisal. *Eur. J. Biochem.* **265**, 698-702
4. Cukier, R. I. (1996) Proton-Coupled Electron Transfer Reactions: Evaluation of Rate Constants. *J. Phys. Chem* **100**, 15428
5. Fagan, R. L., and Palfey, B. A. (2010) Flavin-dependent enzymes. in *Comprehensive Natural Products Chemistry II* (Begley, T. ed.), Elsevier, Oxford, UK. pp 37-114
6. Joosten, V., and van Berkel, W. J. H. (2007) Flavoenzymes. *Curr. Op. Struct. Biol.* **11**, 195-202
7. Willistein, M., Bechtel, D. F., Müller, C. S., Demmer, U., Heimann, L., Kayastha, K., Schünemann, V., Pierik, A. J., Ullmann, G. M., Ermler, U., and Boll, M. (2019) Low

potential enzymatic hydride transfer via highly cooperative and inversely functionalized flavin cofactors. *Nat. Commun.* **10**, 2074

8. Gorelick, R. J., Schopfer, L. M., Ballou, D. P., Massey, V., and Thorpe, C. (1985) Interflavin oxidation-reduction reactions between pig kidney general acyl-CoA dehydrogenase and electron-transferring flavoprotein. *Biochemistry* **24**, 6830-6839
9. Schopfer, L. M., Ludwig, M. L., and Massey, V. (1991) A working proposal for the role of the apoprotein in determining the redox potential of the flavin in flavoproteins: correlations between potentials and flavin pKs. in *Flavins and Flavoproteins 1990* (Curti, B., Ronchi, S., and Zanetti, G. eds.), Walter de Güyter, Berlin. pp 399-404
10. Miura, R. (2001) Versatility and specificity in flavoenzymes: Control mechanisms of flavin reactivity. *Chemical Record* **1**, 183-194
11. Harbury, H. A., and Foley, K. A. (1958) Molecular interaction of isoalloxazine derivatives. *Proc. Natl. Acad. Sci. U. S. A.* **44**, 662-668
12. Harbury, H. A., LaNoue, K. F., Loach, P. A., and Amick, R. M. (1959) Molecular interaction of isoalloxazine dervaties. II. *Proc. Nat. Acad. Sci. U S A* **45**, 1708-1717
13. Macheroux, P., Massey, V., and Thiele, D. J. (1991) Expression of spinach glycolate oxidase in *Saccharomyces cerevisia*e: purification and characterization. *BIochem.* **30**, 4612-4619
14. Chowdhury, N. P., Mowafy, A. M., Demmer, J. K., Upadhyay, V., Koelzer, S., Jayamani, E., Kahnt, J., Hornung, M., Demmer, U., Ermler, U., and Buckel, W. (2014) Studies on the Mechanism of Electron Bifurcation Catalyzed by Electron Transferring Flavoprotein (Etf) and Butyryl-CoA Dehydrogenase (Bcd) of *Acidaminococcus fermentans*. *J. Biol. Chem.* **289**, 5145-5157
15. Schut, G. J., Raseek, N. R., Tokmina-Lukaszewska, M., Mulder, D. E., Nguyen, D. M. N., Lipscomb, G. L., Hoben, J. P., Patterson, A., Lubner, C. E., King, P. W., Peters, J. W., Bothner, B., Miller, A. F., and Adams, M. W. W. (2019) The catalytic mechanism of electron bifurcating electron transfer flavoproteins (ETFs) involves an intermediary complex with NAD+. *J. Biol. Chem.* **293**, ASAP

16. Mohamed-Raseek, N., Duan, H. D., Mroginski, M. A., and Miller, A. F. (2019) Spectroscopic, thermodynamic and computational evidence of the locations of the FADs in the nitrogen fixation-associated electron transfer flavoprotein. *Chemical Sci.* **10**, 7762-7772

17. Sato, K., Nishina, Y., and Shiga, K. (2003) Purification of electron-transferring flavoprotein from Megasphaera elsdenii and binding of additional FAD with an unusual absorption spectrum. *J Biochem* **134**, 719-729

18. Sato, K., Nishina, Y., and Shiga, K. (2013) Interaction between NADH and electron-transferring flavoprotein from *Megasphaera elsdenii*. *J. Biochem.* **153**, 565-572

19. Duan, H. D., Lubner, C. E., Tokmina-Lukaszewska, M., Gauss, G. H., Bothner, B., King, P. W., Peters, J. W., and Miller, A. F. (2018) Distinct flavin properties underlie flavin-based electron bifurcation within a novel electron-transferring flavoprotein FixAB from *Rhodopseudomonas palustris*. *J. Biol. Chem.* **293**, 4688-4701

20. Nitschke, W., and Russell, M. J. (2012) Redox bifurcations: Mechanisms and importance to life now, and at its origin. *Bioessays* **34**, 106-109

21. Peters, J. W., Miller, A. F., Jones, A. K., King, P. W., and Adams, M. W. (2016) Electron bifurcation. *Curr. Opin. Chem. Biol.* **31**, 146–152

22. Frago, S., Goni, G., Herguedas, B., Peregrina, J. R., Serrano, A., Perez-Dorado, I., Molina, R., Gomez-Moreno, C., Hermoso, J. A., Martinez-Julvez, M., Mayhew, S. G., and Medina, M. (2007) Tuning of the FMN binding and oxido-reduction properties by neighboring side chains in Anabaena flavodoxin. *Archives of Biochemistry and Biophysics* **467**, 206-217

23. Sweeney, W. V. (1980) Proteins containing 4Fe-4A clusters: an overview. *Ann. Rev. Biochem.* **49**, 139-161

24. Tagawa, K., and Arnon, D. I. (1968) Oxidation-reduction potentials and stoichiometry of electron transfer in ferredoxins. *Biochim Biophys Acta* **153**, 602-613

25. Herrmann, G., Jayamani, E., Mai, G., and Buckel, W. (2008) Energy conservation via electron-transferring flavoprotein in anaerobic bacteria. *J. Bacteriol.* **190**, 784-791

26. Buckel, W., and Thauer, R. K. (2018) Flavin-based electron bifurcation, a new mechanism of biological energy coupling. *Chem. Rev.* **118**

27. Müller, V., Chowdhury, N. P., and Basen, M. (2018) Electron bifurcation: A long-hidden energy-coupling mechanism. *Annu. Rev. Microbiol.* **72**, 331-353

28. Baymann, F., Schoepp-Cothenet, B., Duval, S., Guiral, M., Brugna, M., Baffert, C., Russell, M. J., and Nitschke, W. (2018) On the natural history of flavin-based electron bifurcation. *Frontiers in Microbiology* **9**, 1357

29. Peters, J. W., Beratan, D. N., Bothner, B., Dyer, R. B., Harwood, C. S., Heiden, Z. M., Hille, R., Jones, A. K., King, P. W., Lu, Y., Lubner, C. E., Minteer, S. D., Mulder, D. W., Raugei, S., J., S. G., Seefeldt, L. C., Tokmina-Lukaszewska, M., Zadvornyy, O. A., Zhang, P., and Adams, M. W. W. (2018) A new era for electron bifurcation. *Curr. Opin. Chem. Biol.* **47**, 32-38

30. Ledbetter, R. N., Garcia Costas, A. M., Lubner, C. E., Mulder, D. E., Tokmina-Lukaszewska, M., Artz, J. H., Patterson, A., Magnuson, T. S., Jay, Z. J., Duan, H. D., Miller, J., Plunkett, M. H., Hoben, J. P., Barney, B. M., Carlson, R. P., Miller, A.-F., Bothner, B., King, P. W., Peters, J. W., and Seefeldt, L. C. (2017) The Electron Bifurcating FixABCX Protein Complex from *Azotobacter vinelandii*: Generation of Low-Potential Reducing Equivalents for Nitrogenase Catalysis. *Biochemistry* **56**, 4177-4190

31. Abramovitz, A. S., and Massey, V. (1976) Interaction of phenols with old yellow enzyme. *J. Biochel. Chem.* **251**, 5327-5336

32. Massey, V., and Palmer, A. G. (1962) Charge transfer complexes of lipoyl dehydrogenase and free flavins. *J. Biol. Chem.* **237**, 2347-2358

33. Dmitrenko, O., Thorpe, C., and Bach, R. D. (2003) Effect of a charge-transfer interaction on the catalytic activity of acyl-CoA dehydrogenase: A theoretical study of the role of oxidized flavin. *J. Phys. Chem. B* **107**, 13229-13236

34. Lin, T.-Y., Werther, T., Jeoung, J.-H., and Dobbek, H. (2012) Suppression of electron transfer to dioxygen by charge transfer and electron transfer complexes in the FAD-dependent reductase component of toluene dioxygenase. *J. Biol. Chem.* **287**, 38338-38346

35. Sakurai, T., and Hosoya, H. (1966) Charge-transfer complexes of nicotinamide-adenine dinucleotide analogues and flavin mononucleotide. *Biochim. Biophys. Acta* **112**, 459-468

36. Koch, M., Breihaoupt, C., Gerhardt, S., Haase, I., Weber, S., Cushman, M., Huber, R., Bacher, A., and Fischer, M. (2004) Structural basis of charge transfer complex formation by riboflavin bound to 6,7-dimethyl-8-ribityllumazine synthase. *Eur. J. Biochem.* **271**, 3208-3214

37. Hardman, S. J. O., Pudney, C. R., Hay, S., and Scrutton, N. S. (2013) Excited state dynamics can be used to probe donor-acceptor distances for H-tunneling reactions catalized by flavoproteins. *Biophys. J.* **105**, 2549-2558

38. Zheng, Y. G., Massey, V., Schaller, A., Palfey, B., A,, and Carey, P. R. (2001) Comparison of resonance Raman spectra of flavin-3,4-dihydroxybenzoate charge-transfer complexes in three flavoenzymes. *J. Raman Spectrosc.* **32**, 579-586

39. Kottke, T., Heberle, J., Hehn, D., Dick, B., and Hegemann, P. (2003) Phot-LOV1: Photocycle of a blue-light receptor domain from the green alga *Chlamydomonas reinhardtii*. *Biophys. J.* **84**, 1192-1201.

40. Gibson, Q. H., Massey, V., and Atherton, N. M. (1962) The nature of compounds present in mixtures of oxidized and reduced flavin mononucleotides. *Biochem. J.* **85**, 369-383

41. Leys, D., Basran, J., Talfournier, F., Sutcliffe, M. J., and Scrutton, N. S. (2003) Extensive conformational sampling in a ternary electron transfer complex. *Nat. Struct. Biol.* **10**, 219-225

42. Toogood, H. S., Leys, D., and Scrutton, N. S. (2007) Dynamics driving function : new insights from electron transferring flavoproteins and partner complexes. *FEBS J.* **274**, 5481-5504

43. Toogood, H. S., van Thiel, A., Scrutton, N., S,, and Leys, D. (2005) Stabilization of non-productive conformations underpins rapid electron transfer to electron transferring flavoprotein. *J. Biol. Chem.* **280**, 30361-30366

44. Demmer, J. K., Bertsch, J., Oppinger, C., Wohlers, H., Kayastha, K., Demmer, U., Ermler, U., and Muller, V. (2018) Molecular basis of the flavin-based electron-bifurcarting caffeyl-coA reductase reaction. *FEBS Lett.* **592**, 332-342

45. Demmer, J. K., Chowdhury, N. P., Selmer, T., Ermler, U., and Buckel, W. (2017) The semiquinone swing in the bifurcating electron transferring flavoprotein/butyryl-coA dehydrogenase complex from *Clostridium difficile*. *Nat. Commun.* **8**, 1577

46. Massey, V. (1991) A simple method for determination of redox potentials. in *Flavins and flavoproteins.* (Curti, B., Ronchi, S., and Zanetti, G. eds.), Walter de Gruyer, Berlin. pp 59-66

47. Xiang, Q., Guo, J., Xu, J., Ding, S., Li, Z., Li, G., Phan, H., Gu, Y., Dang, Y., Xu, Z., Gong, Z., Hu, W., Zeng, Z., Wu, J. F., and Sun, Z. (2020) Stable Olympicenyl Radicals and Their π-Dimers. *J. Am. Chem. Soc.* **142**, 11022-11031

48. Augustin, P., Toplak, M., Fuchs, K., Gerstmann, E. C., Prassl, R., Winkler, A., and Macheroux, P. (2018) Oxidation of the FAD cofactor to the 8-formyl-derivative in human electron-transferring flavoprotein. *J. Biol. Chem.* **293**, 2829-2840

49. Lehman, T. C., and Thorpe, C. (1992) A new form of mammalian electron transfer flavoprotein. *Arch Biochem. Biophys.* **292**, 594-599

50. Geng, J., Dornevil, K., Davidson, V. L., and Liu, A. (2013) Tryptophan-mediated charge-resonance stabilization in the bis-Fe(IV) redox state of MauG. *Proc Natl Acad Sci U S A* **110**, 9639-9644

51. Sato, K., Nishina, Y., and Shiga, K. (1992) The binding of adenine nucleotides to apo-electron-transferring flavoprotein. *J Biochem* **112**, 804-810

52. Sucharitakul, J., Buttranon, S., Wongnate, T., Chowdhury, N. P., Prongjit, M., Buckel, W., and Chaiyen, P. (2020) Modulations of the reduction potentials of flavin-based electron bifurcation complexes and semiquinone stabilities are key to control directional electron flow. *FEBS J.* **ASAP**, doi:10.1111/febs.15343

53. Gray, H. B., and Winkler, J. R. (2015) Hole hopping through tyrosine/tryptophan chains protects proteins from oxidative damage. *Proc Natl Acad Sci U S A* **112**, 10920-10925

54. Warren, J. J., Ener, M. E., Vlcek, A., Jr., Winkler, J. R., and Gray, H. B. (2012) Electron hopping through proteins. *Coord. Chem. Rev.* **256**, 2478-2487

55. Staudt, H., Hoesl, M. G., Dreuw, A., Serdjukow, S., Oesterhelt, D., Budisa, N., Wachtveitl, J., and Grininger, M. (2013) Directed manipulation of a flavoprotein photocycle. *Angew. Chem. Int. Ed.* **52**, 8463-8466

56. Close, D. M. (2011) Calculated vertical ionization energies of the common α-amino acids in the gas phase and in solution. *J. Phys. Chem. A* **115**, 2900-2912

57. Garcia Costas, A. M., Poudel, S., Miller, A.-F., J., S. G., Ledbetter, R. N., Fixen, K., Seefeldt, L. C., Adams, M. W., Harwood, C. S., Boyd, E. S., and Peters, J. W. (2017) Defining Electron Bifurcation in the Electron Transferring Flavoprotein Family. *J. Bacteriol.*

58. Yang, C.-Y. (2006) *The effects of the N(5) hydrogen bond and the re-face positive charge on the redox properties of flavin in the methylotrophic bacterium W3A1 electron transfer flavoprotein.*Ph. D., Ohio State University

59. Gross, E., Sevier, C. S., Heldman, N., Vitu, E., Bentzur, M., Kaiser, C. A., Thorpe, C., and Fass, D. (2006) Generating disulfides enzymatically: reaction products and electron acceptors of the endoplasmic reticulum thiol oxidase Ero1p. *Proc. Natl. Acad. Sci. USA* **103**, 299-304

60. Andersson, D., Freskgard, P.-O., Jonsson, B.-H., and Carlsson, U. (1997) Formation of local native-like tertiary structures in the slow refolding reaction of human carbonic anhydrase II as monitored by circular dichroism on tryptophan mutants. *Biochemistry* **36**, 4623-4630

61. Grajek, H., Gryczynski, I., Bojarski, P., Gryczynski, Z., Bharill, S., and Kulak, L. (2007) Flavin mononucleotide fluorescence intensity decay in concentrated aqueous solutions. *Chem. Phys. Lett.* **439**, 151-156

62. Staudt, H., Oesterhelt, D., Grininger, M., and Wachtveitl, J. (2012) Ultrafast excited-state deactivation of flavins bound to dodecin. *J. Biol. Chem.* **287**, 17637-17644

63. Aliverti, A., Curti, B., and Vanoni, M. A. (1999) Identifying and quantitating FAD and FMN in simple and in iron-sulfur-containing flavoproteins. in *Methods in Molecular Biology* (Chapman, S. K., and Reid, G. A. eds.), Humana Press Inc., Totowa, NJ. pp 9-23

64. Islam, S. D. M., Susdorf, T., Penzkofer, A., and Hegemann, P. (2003) Fluorescence quenching of flavin adenine dinucleotide in aqueous solution by pH dependent isomerisation and photo-induced electron transfer. *Chem. Phys.* **295**, 137-149

65. de Foresta, B., Tortech, L., Vincent, M., and Gallay, J. (2002) Location and dynamics of tryptophan in transmembrane α-helix peptides: a fluorescence and circular dichroism study. *Eur. Biophys. J.* **31**, 185-197

66. Grininger, M., Zeth, K., and Oesterhelt, D. (2006) Dodecins: a family of lumichrome binding proteins. *J. Mol. Biol.* **357**, 842-857

67. Meissner, B., Schleicher, E., Weber, S., and Essen, L.-O. (2007) The dodecin from *Thermus thermophilus*, a bifunctional cofactor storage protein. *J. Biol. Chem.* **282**, 33142-33154

68. Brisker-Klaiman, D., and Dreuw, A. (2019) On the influence of dimerisation of lumiflavin in aqueous solution on its optical spectra – a quantum chemical study. *Mol. Phys.* **117**, 2167-2178

69. D'Alessandro, D. M., and Keene, F. R. (2006) Current trends and future challenges in the experimental, theoretical and computational analysis of intervalence charge transfer (IVCT) transitions. *Chem. Soc. Rev.* **35**, 424-440

70. Sorokin, A. V., Ropakova, I. Y., Wolter, S., Lange, R., Barke, I., Speller, S., Yefimova, S. L., Malyukin, Y. V., and Lochbrunner, S. (2019) Exciton dynamics and self-trapping of carbocyanine J-aggregates in polymer films. *J. Phys. Chem. C* **123**, 9428-9444

71. Lostao, A., Gomez-Moreno, C., Mayhew, S. G., and Sancho, J. (1997) Differential stabilization of the three FMN redox forms by tyrosine 94 and tryptophan 57 in flavodoxin from *Anabaena* and its influence on the redox potentials. *Biochemistry* **36**, 14334-14344

72. Dunn, R. V., Munro, A. W., Turner, N. J., Rigby, S. E. J., and Scrutton, N., S,. (2010) Tyrosyl radical formation and propagation in flavin dependent monoamine oxidases. *Chem. Bio. Chem.* **11**, 1228-1231

73. McCormick, D. B., Li, H.-C., and MacKenzi, R. E. (1967) Spectral evidence for interaction of riboflavin with aromatic hydrocarbons. *Spectrochim. Acta* **23A**, 2353-2358

74. He, T.-F., Guo, L., Guo, X., Chang, C.-W., Wang, L., and Zhong, D. (2013) Femtosecond Dynamics of Short-Range Protein Electron Transfer in Flavodoxin. *Biochemistry* **52**, 9120-9128

75. Hopkins, N., and Stanley, R. J. (2003) Measurement of the electronic properties of the flavoprotein old yellow enzyme (OYE) and the OYE:p-Cl phenol charge-transfer complex using Stark spectroscopy. *Biochem.* **42**, 991-999

76. Rietveld, P., Arscott, L. D., Berry, A., Scrutton, N., S,, Deonarian, M. P., Perham, r. N., and Williams, J., C. H. (1994) Reductive and oxidative half-reactions of glutathione reductase from Escherichia coli. *Biochemistry* **33**, 13888-13895

77. Schaefer-Ramadan, S., Thorpe, C., and Rozovsky, S. (2014) Site-specific insertion of selenium into the redox-active disulfide of the flavoprotein augmenter of liver regeneration. *Arch Biochem. Biophys.* **548**, 60-65

78. Swenson, R. P., and Krey, G. D. (1994) Site-directed mutagenesis of Tyrosine-98 in the flavodoxin from *Desulfovibrio vulgaris* (Hildenborough): Regulation of the oxidation-reduction properties of the bound FMN cofactor by aromatic, solvent and electrostatic interactions. *Biochemistry* **33**, 8505-8514

79. Monaco, H. L. (1997) Crystal Structure of Chicken Riboflavin-Binding Protein. *EMBO J.* **16**, 1475−1483

80. Grininger, M., Staudt, H., Johansson, P., Wachtveitl, J., and Oesterhelt, D. (2009) Dodecin Is the Key Player in Flavin Homeostasis of Archaea. . *J. Biol. Chem.* **284**, 13068−13076

81. Muralidhara, B. K., and Wittung-Strafshede, P. (2003) Can cofactor-binding sites in proteins be flexible? Desulfovibrio desulfuricans flavodoxin binds FMN dimer. *Biochemistry* **42**, 13074-13080

82. Drew, H. R., Wing, R. M., Takano, T., Broka, C., Tanaka, S., Itakura, K., and Dickerson, R. E. (1981) Structure of a B-DNA dodecamer: conformation and dynamics. *Proc. Nat. Acad. Sci. U S A* **78**, 2179-2183

83. Grajek, H., Drabent, R., Zurkowska, G., and Bojarski, C. (1984) Absorption of the flavin dimers. *Biochim. Biophys. Acta* **801**, 456-460

84. Ju, S. Y., and Papadimitrakopoulos, F. (2008) Synthesis and redox behavior of flavin mononucleotide-functionalized single-walled carbon nano- tubes. *J. Am. Chem. Soc.* **130**, 655-664

85. Breinlinger, E. C., and Rotello, V. M. (1997) Model systems for flavoenzyme activity. Modulation of flavin redox potentials through Pi-stacking interactions. *J. Am. Chem. Soc.* **119**, 1165-1166

86. Bresnahan, C. G., Reinhardt, C. R., Bartholow, T. G., Rumpel, J. P., North, M. A., and Bhattacharyya, S. (2014) Effect of stacking interactions on the thermodybamics and kinetics of lumiflavin: a study with improved density functionals and density functional tight-binding protocol. *J. Phys. Chem. A* **119**, 172-182

87. Grajek, H. (2003) The effect of temperature on FMN absorption spectra in rigid poly(vinyl alcohol) matrices. *Biochim. Biophys. Acta* **1620**, 133-138

88. Isenberg, I., and Szent-Györgyi, A. (1959) On charge transfer complexes between substances of biochemical interest. *Proc. Nat. Acad. Sci. U S A* **45**, 1229-1231

89. Beinert, H. (1956) Spectral characteristics of flavins at the semiquinoid oxidation level. *J. Am. Chem. Soc.* **78**, 5323-5328

90. Michaelis, L., and Schwarzenbach, G. (1938) The intermediate forms of oxidation-reduction of the flavins. *J. Biol. Chem.* **123**, 527-542

91. Ehrenberg, A., Müller, F., and Hemmerich, P. (1967) Basicity, visible spectra an delectron spin resonance of flavosemiquinone anions. *Eur J. Biochem.* **2**, 282-293

92. Gruber, T. D., Dimond, M. C., Kiessling, L. L., and Forest, K. T. (2009) Structure of UDP-galactopyranose mutase bound to flavin mononucleotide. *RCSB PDB* **3KYB.pdb**

93. Nissen, M. S., Youn, B., Knowles, B. D., Ballinger, J. W., Jun, S.-Y., Belchik, S. M., Xun, L., and Kang, C. (2008) Crystal structures of NADH:FMN oxidoreductase (EmoB) at different stages of catalysis. *J. Biol. Chem.* **283**, 28710-28720

94. McNamara, D. E., Cascio, D., Jorda, J., Bustos, C., Wang, T.-C., Rasche, M. E., Yeates, T. O., and Bobik, T. A. (2014) Structure of dihydromethanopterin reductase, a cubic protein cage for redox transfer. *J. Biol. Chem.* **289**, 8852-8864

95. Hu, J., Chuenchor, W., and Rokita, S. E. (2015) A Switch between One- and Two-electron Chemistry of the Human Flavoprotein Iodotyrosine Deiodinase Is Controlled by Substrate. *J. Biol. Chem.* **290**, 590-600

96. Edelhoch, H. (1967) Spectroscopic determination of tryptophan and tyrosine in proteins. *Biochemistry* **6**, 1948-1954

97. Whitby, L. G. (1953) A new method for preparing flavin-adenine dinucleotide. *The Biochemical journal* **54**, 437-442

98. Bock, R. M., Ling, N. S., Morell, S. A., and Lipton, S. H. (1956) Ultraviolet absorption spectra of adenosine-5'-triphosphate and related 5'-ribonucleotides. *Arch Biochem Biophys* **62**, 253-264

99. Mayhew, S. G. (1978) The redox potential of dithionite and SO-2 from equilibrium reactions with flavodoxins, methyl viologen and hydrogen plus hydrogenase. *Eur. J. Biochem.* **85**, 535-547

100. Haid, E., Lehmann, P., and Ziegenhorn, J. (1975) Molar absorptivities of beta-NADH and beta-NAD at 260 nm. *Clinical chemistry* **21**, 884-887

101. Frisch, M. J., Trucks, G. W., Schlegel, H. B., Scuseria, G. E., Robb, M. A., Cheeseman, J. R., Scalmani, G., Barone, V., Petersson, G. A., Nakatsuji, H., Li, X., Caricato, M., Marenich, A. V., Bloino, J., Janesko, B. G., Gomperts, R., Mennucci, B., Hratchian, H. P., Ortiz, J. V., Izmaylov, A. F., Sonnenberg, J. L., Williams-Young, D., Ding, F., Lipparini, F., Egidi, F., Goings, J., Peng, B., Petrone, A., Henderson, T., Ranasinghe, D., Zakrzewski, V. G., Gao, J., Rega, N., Zheng, G., Liang, W., Hada, M., Ehara, M., Toyota, K., Fukuda, R., Hasegawa, J., Ishida, M., Nakajima, T., Honda, Y., Kitao, O., Nakai, H., Vreven, T., Throssell, K., Montgomery, J. A., Jr., Peralta, J. E., Ogliaro, F., Bearpark, M. J., Heyd, J. J., Brothers, E. N., Kudin, K. N., Staroverov, V. N., Keith, T. A., Kobayashi, R., Normand, J., Raghavachari, K., Rendell, A. P., Burant, J. C., Iyengar, S. S., Tomasi, J., Cossi, M., Millam, J. M., Klene, M., Adamo, C., Cammi, R., Ochterski, J. W., Martin, R. L., Morokuma, K., Farkas, O., Foresman, J. B., and Fox, D. J. (2016) Gaussian 16, Revision B.01. *Gaussian, Inc.,* **Wallingford, CT**

102. Cossi, M., Rega, N., Scalmani, G., and Vincenzo, B. (2003) Energies, structures, and electronic properties of molecules in solution with the C-PCM solvation model. *J. Comput. Chem.* **24**, 669-681

103. Yanai, T., Tew, D. P., and Handy, N. C. (2004) A new hybrid exchange-correlation functional using the Coulomb-attenuating method (CAM-B3LYP). *Chem. Phys. Lett.* **393**, 51-57

104. Karasulu, B., Götze, J. P., and Thiel, W. (2014) Vibrationally broadened UV-vis absorption spectra of flavin derivatives: riboflavin, roseoflavin, and 5-thioflavin. *J. Chem. Theor. Comp.* **10**, 5549-5566

105. Chai, J.-D., and Head-Gordon, M. (2008) Long-range corrected hybrid density functionals with damped atom-atom dispersion corrections. *Phys. Chem. Chem. Phys.* **10**, 6615-6620

106. Dunning, T. H., Jr. (1989) Gaussian Basis Sets for the Use in Correlated Molecular Calculations, I: The Atoms Boron Through Neon and Hydrogen. *J. Chem. Phys.* **90**, 1007-1023

107. Hariharan, P. C., and Pople, J. A. (1973) The influence of polarization functions on molecular orbital hydrogenation energies. *Theor. Chim. Acta* **28**, 213-222

108. Jacquemin, D., Wathelet, V., Perpete, E. A., and Adamo, C. (2009) Extensive TD-DFT benchmark: singlet-excited states of organic molecules. *J. Chem. Theory Comp.* **5**, 2420-2435

109. Dreuw, A., and Head-Gordon, M. (2005) Single-reference ab initio methods for the calculation of excited states of large molecules. *Chem. Rev.* **105**, 4009-4037

110. Gaussian. (2017) Creating UV/Visible plots from the results of excited states calculations., Gaussian

111. DeLano, W. L. (2002) The PyMOL Molecular Graphics System. http://www.pymol.org **DeLano Scientific**

112. Pettersen, E. F., Goddard, T. D., Huang, C. C., Couch, G. S., Greenblatt, D. M., Meng, E. C., and Ferrin, T. E. (2004) UCSF Chimera - a visualization system for exploratory research and analysis. *J. Comput. Chem.* **25**, 1605-1612

113. Dennington, R., Keith, T. A., and Millam, J. M. (2016) GaussView, Version 6. *Semichem Inc., Shawnee Mission, KS*

114. Robbins, J. M., Souffrant, M. G., Hamelberg, D., Gadda, G., and Bommarius, A. S. (2018) Enzyme-mediated conversion of flavin adenine dinucleotide (FAD) to 8-formyl FAD in formate oxidase results in a modified cofactor with enhanced catalytic properties. *Biochem* **56**, 3800-3807

Figures

Figure 1

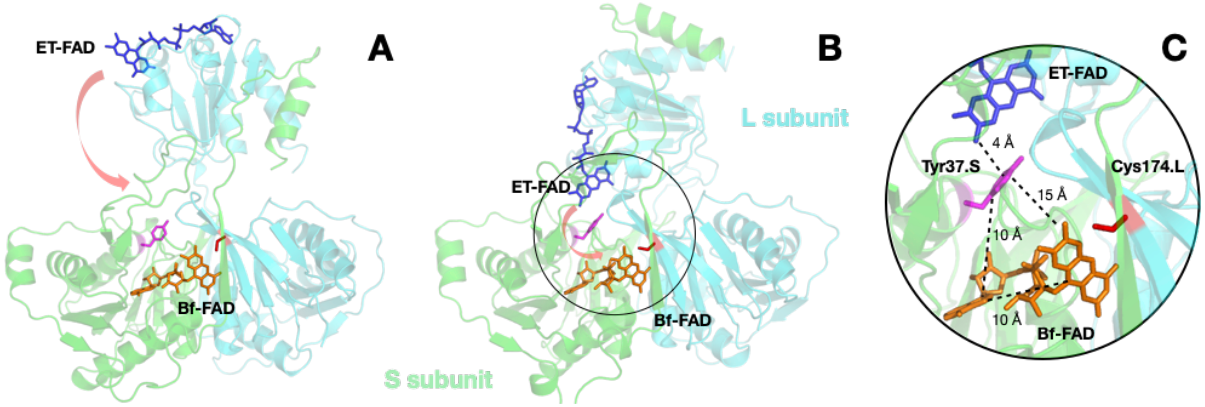

Figure 1. Structural models of *Rpa*ETF showing the D conformation (A) and B-like conformation (B). The large (L) subunit, also known as the ETFα or FixB subunit is shown in cyan and the small (S) subunit, also known as the ETFβ or FixA subunit is shown in green. Bf-FAD and ET-FAD are shown in orange and blue, respectively. Conserved residues Tyr37.S and Cys174.L are shown in magenta and red, respectively. The electron-donating conformation (D conformation (45)) structure is modeled onto the structure of *Acetobacterium woodii* caffeyl-CoA reductase-associated Bf-ETF (*Awo*CarCDE: 6FAH.pdb (44)) while the bifurcating-like (B-like) conformation structure is modeled onto the *Acidaminococcus fermentans* Bf-ETF (*Afe*ETF: 4KPU.pdb (14)). The large red arrow in (A) depicts the rotation of of the head domain to form the B-like conformation in (B), while the small red arrow in (B) shows further head domain rotation required to form the *bona fide* B conformation in which we propose that the two flavins are brought into van der Waals contact.

Figure 2

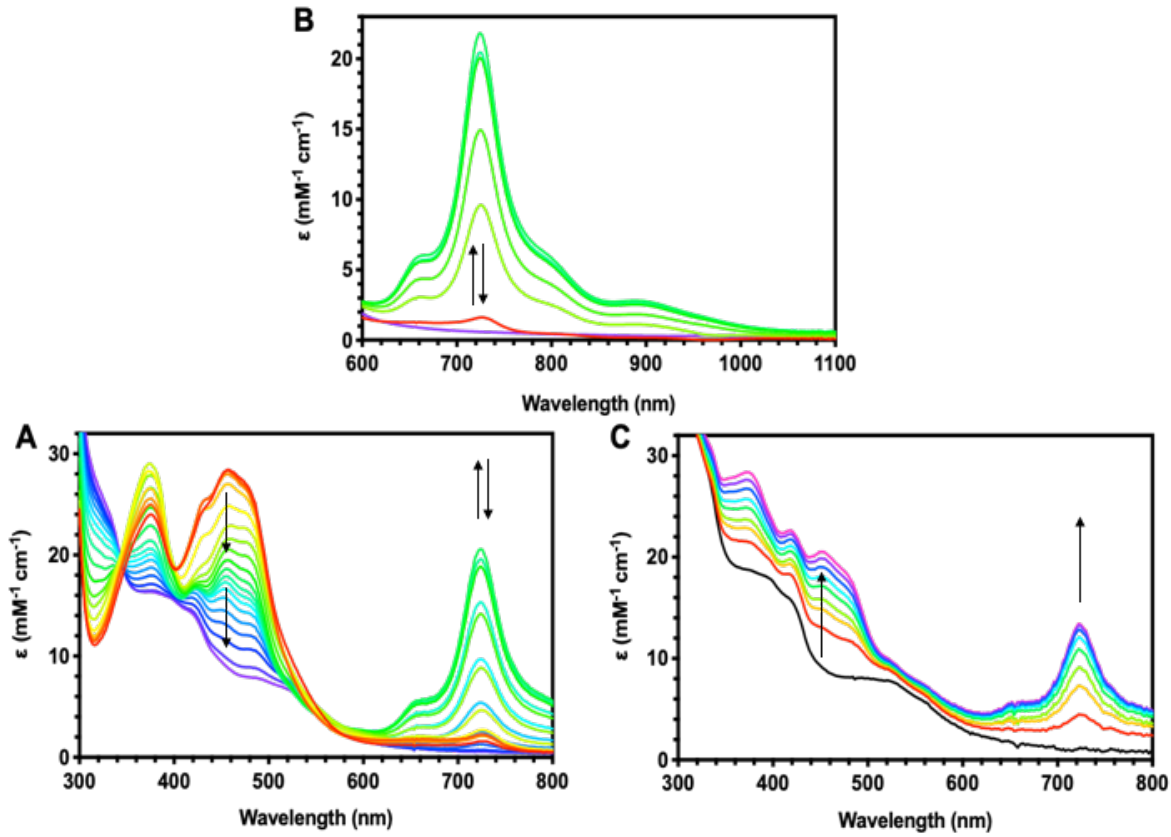

Figure 2. Formation and reversibility of the 726 nm species in WT *Rpa*ETF. (A) Reductive titration of WT *Rpa*ETF (68.7 µM) by 3.42 mM sodium dithionite at pH 9.0. (B) Long-wavelength spectra corresponding to the starting fully oxidized *Rpa*ETF (red), the same sample half-reduced and successive spectra obtained in the course of stepwise reduction by dithionite to the fully reduced endpoint (purple). (C) Titration of fully dithionite-reduced WT *Rpa*ETF (13.9 µM) by 2.78 mM NAD^+ at pH 9.0. All titrations are done in 20 mM bis-Tris propane, pH 9.0, 200 mM KCl, 10% (w/v) glycerol.

Figure 3

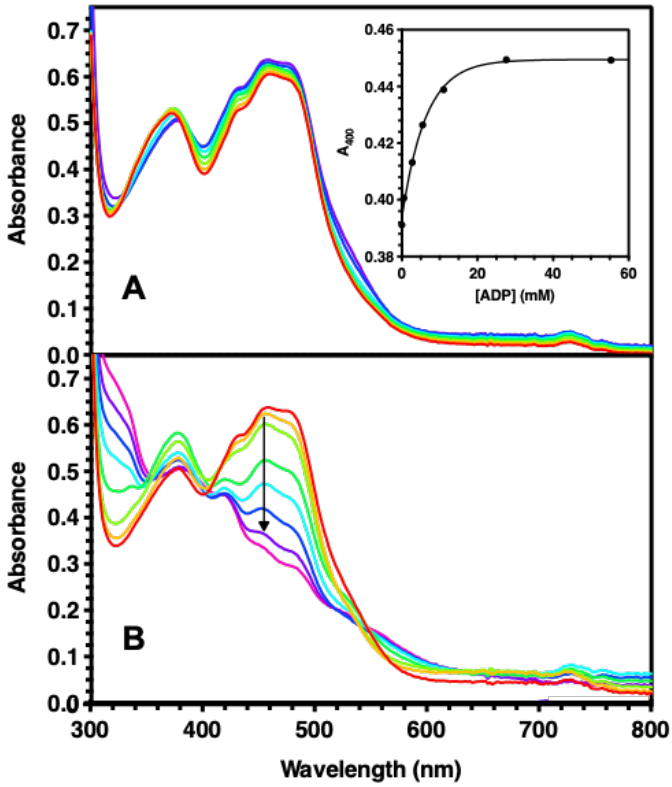

Figure 3. Reductive titration of WT *Rpa*ETF from which the ET-FAD was displaced by ADP. (A) Displacement of ET-FAD monitored via UV-visible spectra of WT *Rpa*ETF (22.2 μM) in the presence of 0 mM, 0.55 mM, 2.77 mM, 5.53 mM, 11.07 mM, 27.67 mM, 55.34 mM ADP (red to purple). Inset also shows the absorbance at 400 nm versus ADP concentration, with a curve provided to guide the eye. (B) Reductive titration of ET-FAD-depleted *Rpa*ETF (22.2 μM) by 3.32 mM sodium dithionite at pH 9.0. Compare with Figure 2A.

Figure 4

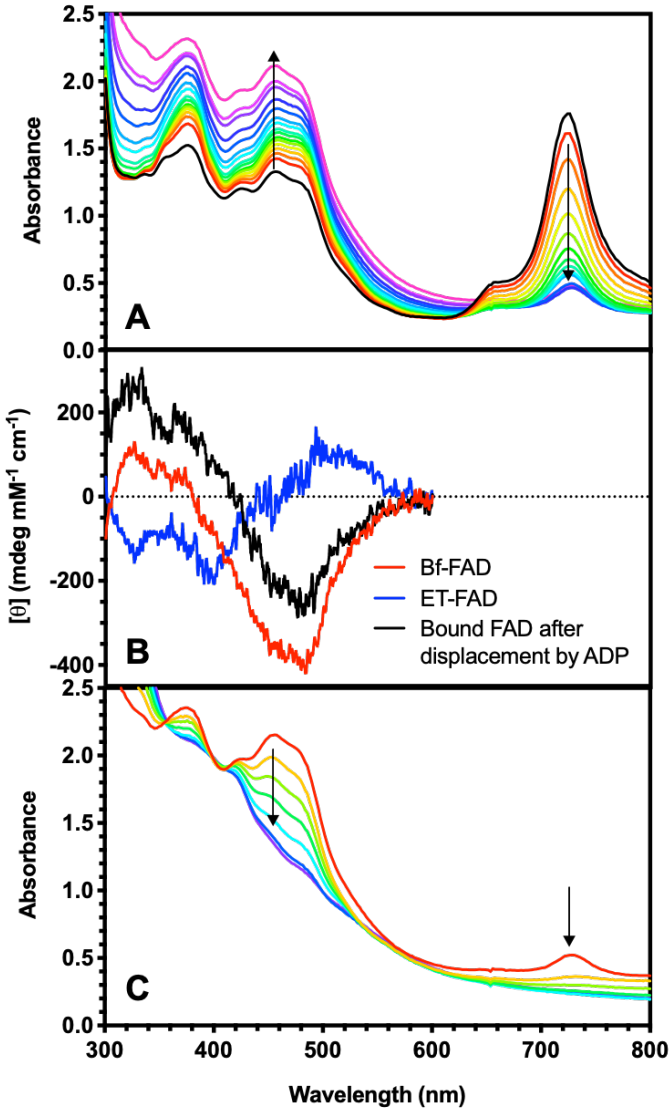

Figure 4. Displacement of FAD by ADP in the half-reduced state WT *Rpa*ETF. (A) UV-visible spectra of half-reduced WT *Rpa*ETF (68.7 µM, black trace) and effect of titration to 0 mM, 1.59 mM, 3.19 mM, 4.78 mM, 6.37 mM, 7.97 mM, 9.56 mM, 11.16 mM, 12.75 mM, 14.34 mM, 15.94 mM, 23.91 mM, 39.84 mM, 63.75 mM, 95.62 mM and 159.37 mM ADP (black to pink). (B) Identification of bound FAD by CD after FAD displacement in half-reduced protein (black trace). For comparison, the CD spectrum of Bf-FAD seen in half-reduced *Rpa*ETF is shown (red trace) along with that of ET-FAD (blue trace) obtained by subtraction of the Bf-FAD CD spectrum from the native protein CD spectrum made up of both Bf-FAD and ET-FAD. (C) Resumed reductive titration of the half-reduced WT *Rpa*ETF (68.7 µM) after FAD displacement, by 3.42 mM sodium dithionite at pH 9.0. All samples were in 20 mM bis-Tris propane, pH 9.0, 200 mM KCl, 10% (w/v) glycerol.

Figure 5

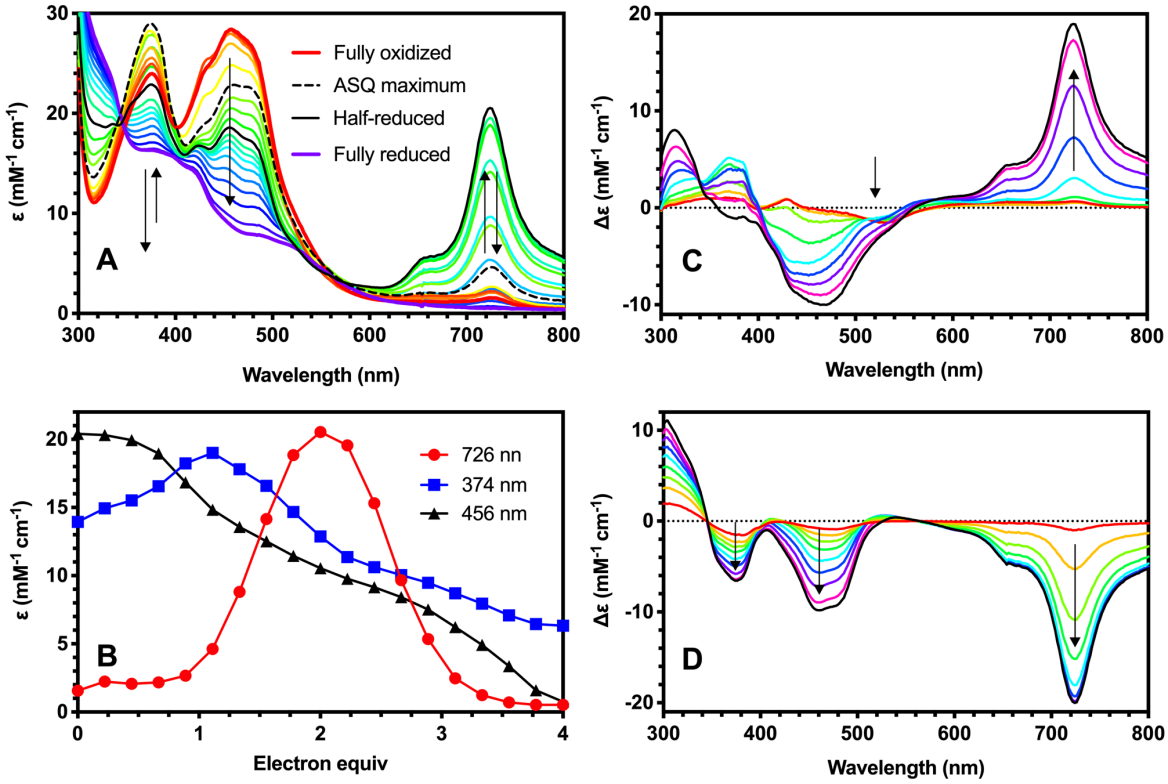

Figure 5. Flavin oxidation state changes associated with formation of the 726 nm species. (A) Reductive titration of WT *Rpa*ETF (68.7 µM) by 3.42 mM sodium dithionite at pH 9.0 showing fully oxidized state (red trace), ASQ maximum (dashed black trace), half-reduced state (solid black trace) and fully reduced state (purple trace). (B) Amplitudes of the 726 nm species, sum of ASQ and OX (as amplitude at 374 nm), and OX species (as amplitude at 456 nm) versus electron equivalents provided, based on (A). (C) Difference spectra (observed spectrum – fully oxidized state spectrum) showing spectral changes that accompany formation of the 726 nm species. Only spectra collected in the course of 726 nm species formation are included. The difference spectrum with the maximum amount of 726 nm species is shown in black. Formation of the 726 nm species is associated with loss of ASQ based on negative absorbance changes at 520 nm. (D) Difference spectra (observed spectrum – 726 nm species maximum spectrum) showing spectral changes that accompany consumption of the 726 nm species. The difference spectrum resulting from the final spectrum is shown in black. Loss of 726 nm species is associated with loss of an OX flavin based on changes at 460 and 370 nm.

Figure 6

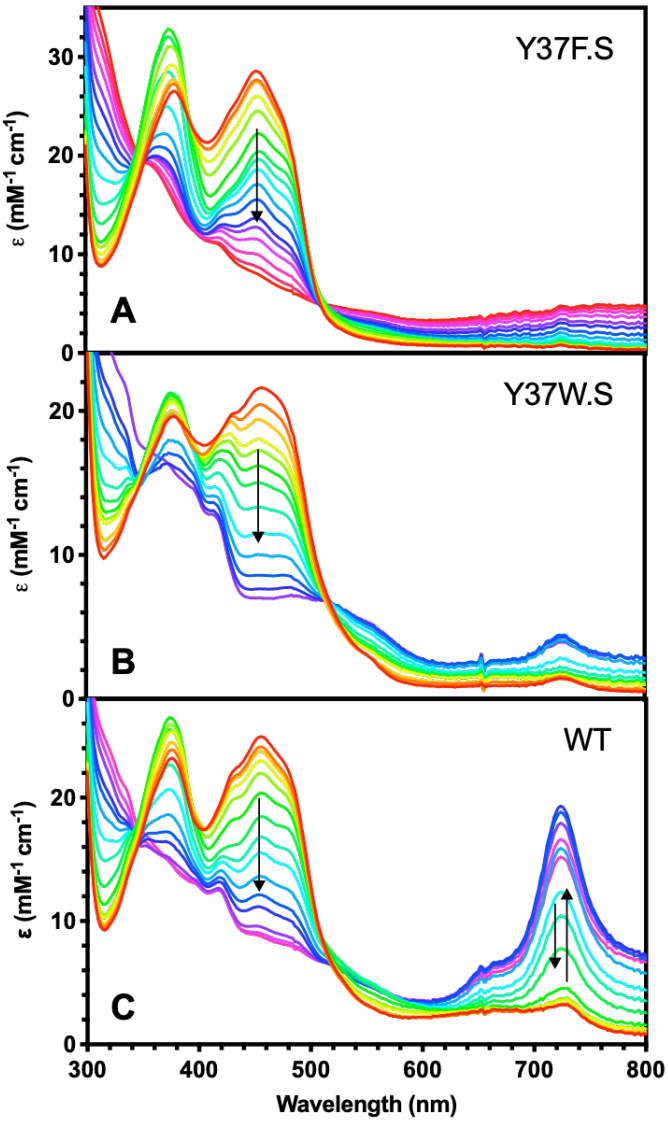

Figure 6. Effect of substitutions of Tyr37.S on the 726 nm species. (A) Reductive titration of Y37F.S *Rpa*ETF (29.9 µM) by 1.50 mM NADH at pH 9.0. (B) Reductive titration of Y37W.S *Rpa*ETF (15.9 µM) by 0.65 mM NADH at pH 9.0. (C) Reductive titration of WT *Rpa*ETF (21.3 µM) by 1.22 mM NADH at pH 9.0. All titrations were done in 20 mM bis-Tris propane, pH 9.0, 200 mM KCl, 10% (w/v) glycerol. For the Y37W.S variant (B), the vertical axis extinction coefficients were calculated on the basis of protein concentration, but this variant contained only 1.2 flavins/ETF vs. 2 for WT (supporting Table S1). A flavin signal amplitude only 60% that of WT is therefore expected for signals reflecting individual flavins. Given evidence that the 726 nm band arises from a pair of flavins, two limiting cases should be considered. In the case of random FAD distribution between the two sites, 36% of ETF heterodimers would possess both FADs and display the 726 nm band. Considering that the Bf site binds oxidized FAD more tightly (17), then only 20% of the ET sites likely contain FAD, making the 726 nm species possible in 20% of dimers. This latter case is more consistent with the observed amplitude indicating that approximately 15% of the dimers form 726 nm species. In comparison, WT forms 726 nm species in 60% of the dimers when titrated with NADH (panel C) similar to its formation in 65 % of ETF dimers when titrated with dithionite, based on the maximum A_{726} obtained (supporting Table S1).

Figure 7

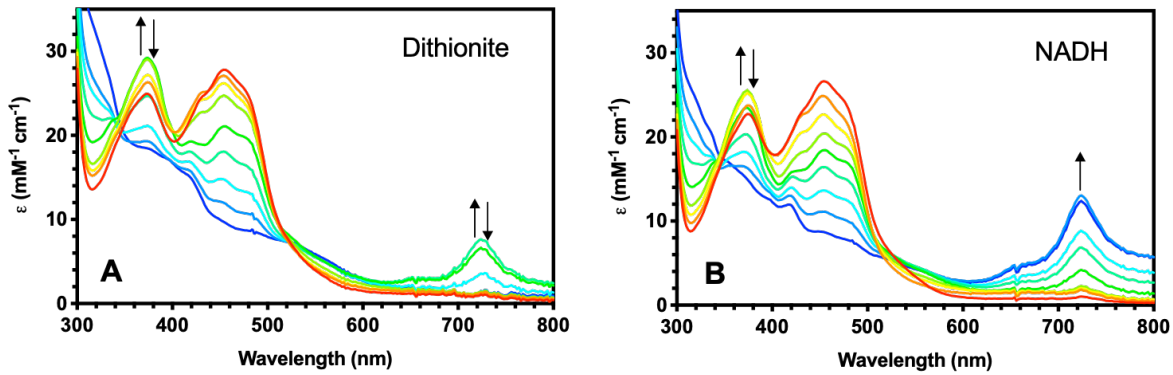

Figure 7. Effect of substitution of C174.L on the 726 nm species. (A) Reductive titration of C174A.L *Rpa*ETF (20.0 μM) by 2.00 mM sodium dithionite at pH 9.0. Analogous WT results are in Figure 2A. (B) Reductive titration of C174A.L *Rpa*ETF (27.4 μM) by 2.74 mM NADH at pH 9.0. Analogous WT titration is in Figure 6C. All titrations were done in 20 mM bis-Tris propane, pH 9.0, 200 mM KCl, 10% (w/v) glycerol. Based on the maximal amplitude at 726 nm C174A.L *Rpa*ETF formed the 726 nm species in 24 % of dimers during titration with dithionite, and in 41% of dimers during titration with NADH.

Figure 8

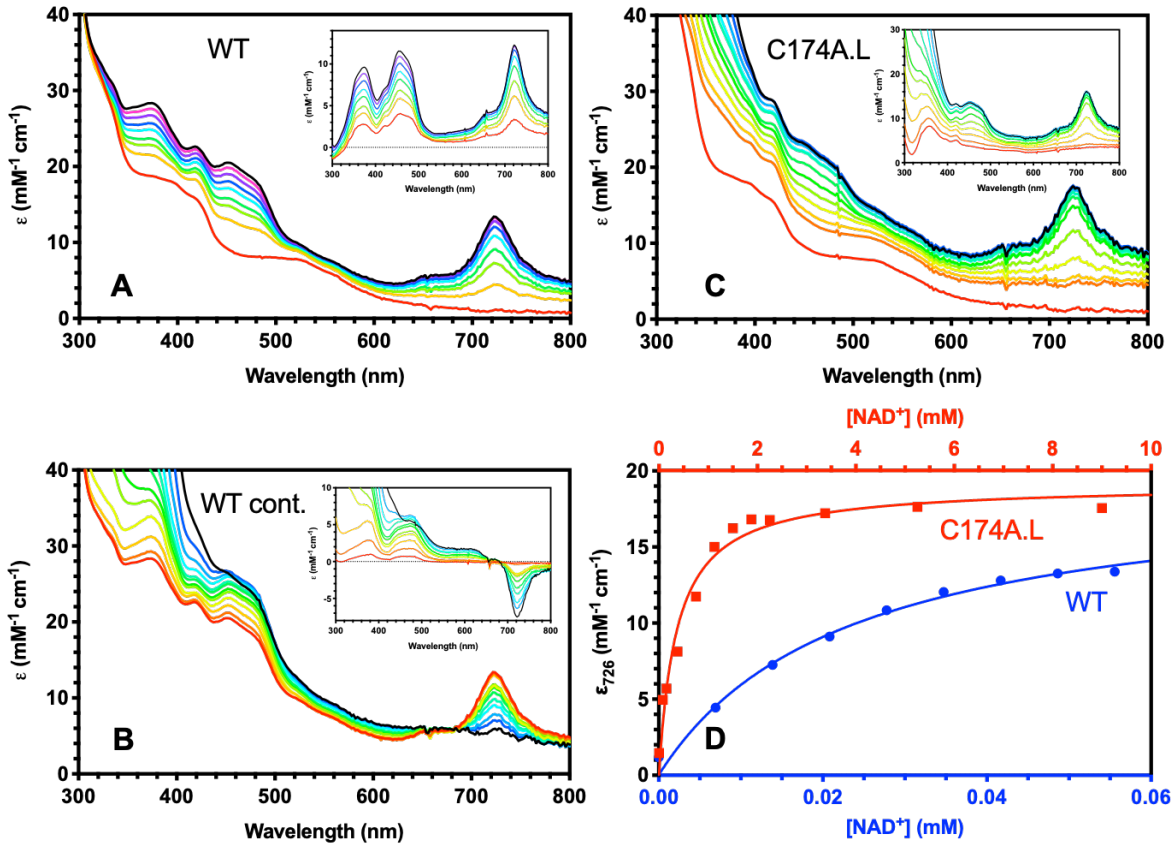

Figure 8. Reversibility of the 726 nm species in WT *Rpa*ETF and C174A.L variant. (A) Titration of fully reduced (via dithionite) WT *Rpa*ETF (13.9 µM) by 2.78 mM NAD^+ at pH 9.0, with inset showing difference spectra (observed spectrum – fully reduced state spectrum) revealing formation of the 726 nm species and OX flavin at 460 and 370 nm (726 nm species maximum shown in black trace) as well as formation of NADH (340 nm) on top of consumption of HQ flavin in the same spectral region. (B) Further titration of the resulting sample from (A) by 139.00 mM NAD^+, with inset showing difference spectra (Observed spectrum – spectrum containing maximal 726 nm species) revealing disappearance of the 726 nm species and formation of more OX flavin at 460 nm (726 nm species minimum shown in black trace). NADH formation is also evident from increasing absorbance at 340 nm. (C) Titration of fully reduced (via dithionite) C174A.L variant (20.0 µM) by 3 mM NAD^+ (from 2nd to 6th trace) and then 150 mM NAD^+ (from 7th to the last black trace) at pH 9.0, with inset showing difference spectra (observed spectrum – fully reduced starting spectrum). These document formation of the 726 nm species in conjunction with OX flavin (726 nm species maximum shown in black trace). All titrations were done in 20 mM bis-Tris propane, pH 9.0, 200 mM KCl, 10% (w/v) glycerol. (D) Estimation of NAD^+ dissociation constant for WT *Rpa*ETF (blue) and C174A.L variant (red). Based on fits to the data of $y = y_{max} \bullet c/(K_d + c)$, an apparent K_d of 0.023 mM was obtained for WT while for C174A.L the obtained apparent K_d was 0.37 mM. Note that these are not strictly dissociation constants as NAD^+ reacts as well as binds. However given the similar *E*°s of the WT and C174A.L *Rpa*ETFs, their reactivities appear similar allowing us to interpret the *change* in apparent K_d in terms of binding. It appears that binding is 15 times weaker in C174A.L than in WT.

Figure 9

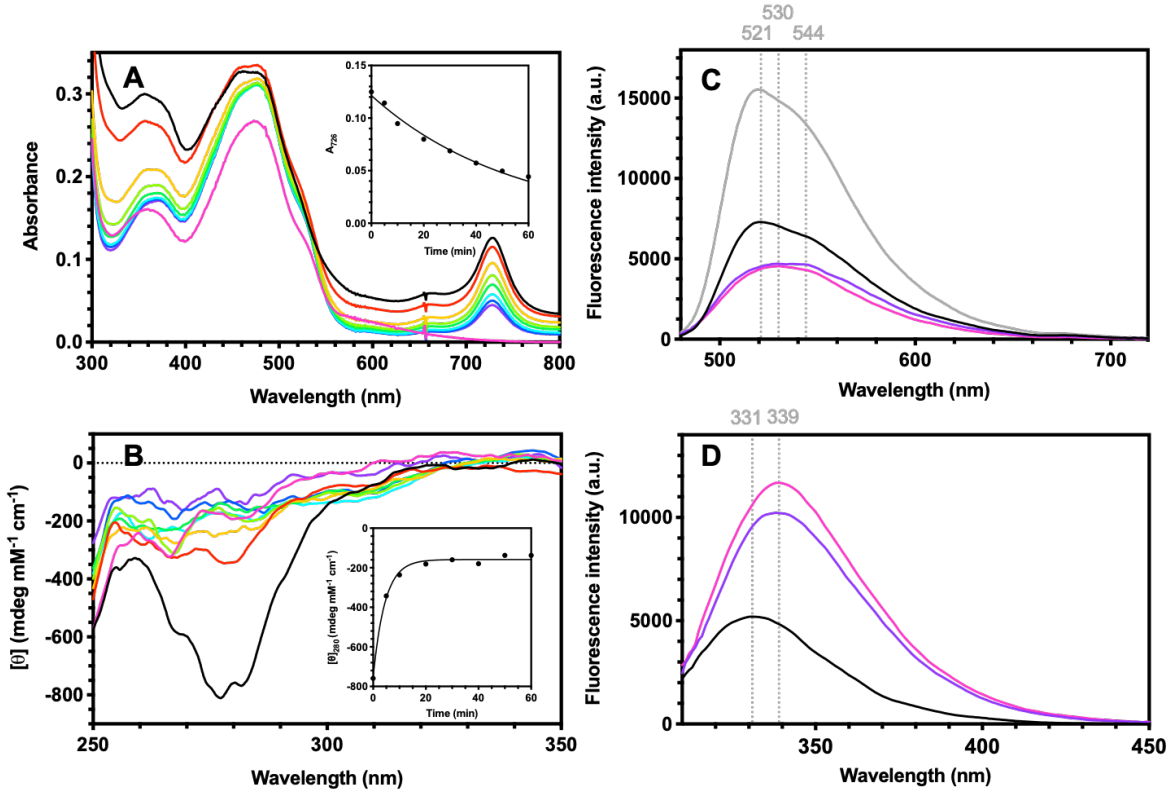

Figure 9. Persistence of the 726 nm species in *Rpa*ETF treated with CTAB. (A) Time course of anaerobic treatment of WT *Rpa*ETF (9.96 μM) bearing the 726 nm species (black trace) in 10 mM CTAB, showing spectra after 5 min (red), 10 min (orange), 20 min (lime), 30 min (green), 40 min (cyan), 50 min (blue), 60 min (purple) and then final treatment with heat aerobically (magenta). Inset shows amplitude of 726 nm band as a function of CTAB treatment time. Amplitudes were fit to a single exponential decay in time. A shoulder around 520 nm persisted in the absorbance spectrum collected after heat-denaturation and the short-wavelength maximum was shifted to 360 nm vs 375 for authentic FAD consistent with possible modification of some of the flavin (48,114). (B) Near-UV CD spectra of the same sample as described in (A) with inset showing time course of tertiary structural change based on molar ellipticity at 280 nm. Negative amplitudes were fit to a single exponential decay in time. (C) Fluorescence emission spectra of FAD in native *Rpa*ETF in the absence of the 726 nm species (ET_{OX}/Bf_{OX}, gray), bearing the 726 nm species before treatment with CTAB (black, presumed ET_{HQ}/Bf_{OX}), vs. after 60 min treatment with CTAB (purple) and after final aerobic heat treatment (magenta). Excitation was at 466 nm. (D) Fluorescence emission spectra of tryptophan excited at 295 nm for *Rpa*ETF bearing the 726 nm species before treatment with CTAB (black), after 60 min treatment with CTAB (purple) and after further heat treatment (magenta).

Figure 10

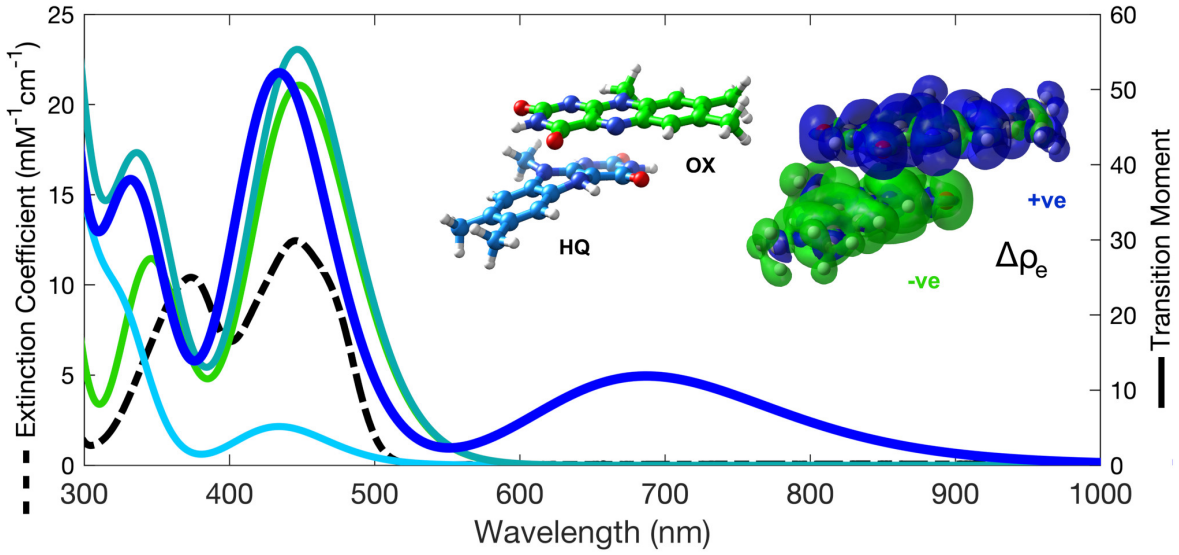

Figure 10. Computed spectra of HQ lumiflavin (LF) (light blue), OX LF (green), sum of HQ LF and OX LF (teal), and LF_{HQ}•LF_{OX} dimer (dark blue) compared with the experimental spectrum of FMN in water (dashed black line). The left vertical axis applies to the experimental spectrum of FMN and the right vertical axis applies to the computed spectra of lumiflavin models. The ball and stick structure shows the geometry-optimized structure of the LF_{HQ}•LF_{OX} dimer where LF_{HQ} is in light blue and LF_{OX} is in green. The starting structure was based on the stacked flavin dimer of *T. thermophilus* dodecin; geometry optimization and TD-DFT calculations employed the cam-B3LYP functional with the cc-pVDZ basis (see Methods). The electron density displacement map corresponding to the long-wavelength transition exclusive to the LF_{HQ}•LF_{OX} dimer was generated with an isovalue of 0.0004 electron density lost (green) and gained (blue) and is displayed on the same structure. The clear net transfer of electron density classifies the transition as a CT transition. Computed absorption maxima incorporate a 0.55 eV red shift to optimize agreement with the 446 nm band of FMN.